REPORT DOCUMENTATION PAGE

Form Approved
OMB NO. 0704-0188

1. AGENCY USE ONLY *(Leave blank)*	2. REPORT DATE	3. REPORT TYPE AND DATES COVERED
		Reprint

4. TITLE AND SUBTITLE

TITLE ON REPRINT

5. FUNDING NUMBERS

DAAG55-98-1-0464

6. AUTHOR(S)

AUTHOR(S) ON REPRINT

7. PERFORMING ORGANIZATION NAMES(S) AND ADDRESS(ES)

Rensselaer Polytechnic Institute

8. PERFORMING ORGANIZATION REPORT NUMBER

9. SPONSORING / MONITORING AGENCY NAME(S) AND ADDRESS(ES)

U.S. Army Research Office
P.O. Box 12211
Research Triangle Park, NC 27709-2211

10. SPONSORING / MONITORING AGENCY REPORT NUMBER

ARO 38324.3-EG

11. SUPPLEMENTARY NOTES

The views, opinions and/or findings contained in this report are those of the author(s) and should not be construed as an official Department of the Army position, policy or decision, unless so designated by other documentation.

12a. DISTRIBUTION / AVAILABILITY STATEMENT

Approved for public release; distribution unlimited.

12 b. DISTRIBUTION CODE

13. ABSTRACT *(Maximum 200 words)*

ABSTRACT ON REPRINT

14. SUBJECT TERMS	15. NUMBER IF PAGES
	16. PRICE CODE

17. SECURITY CLASSIFICATION OR REPORT	18. SECURITY CLASSIFICATION OF THIS PAGE	19. SECURITY CLASSIFICATION OF ABSTRACT	20. LIMITATION OF ABSTRACT
UNCLASSIFIED	UNCLASSIFIED	UNCLASSIFIED	UL

1.14 Micromechanics of Inelastic Composite Materials

YEHIA A. BAHEI-EL-DIN
Cairo University, Giza, Egypt
and
GEORGE J. DVORAK
Rensselaer Polytechnic Institute, Troy, NY, USA

1.14.1 INTRODUCTION

Design of composite aggregates for a specific application involves several physical and geometrical parameters related to the micro-structure, and depends on the type of service loads and the application environment. Moreover, fabrication methods and parameters cause significant local stresses and deformation that may affect the performance of the material.

Under these circumstances, it is essential to develop micromechanical theories which evaluate the local fields and predict the overall response under combined thermal and mechanical loads. The basic elements of these theories are geometrical modeling of the microstructures and local interactions, and constitutive modeling of the homogeneous phases. An essential requirement of the latter is to include inelastic deformation to model composite systems which exhibit nonlinear response under thermal and mechanical service loads.

Since the early 1960s, micromechanics of composite materials has attracted many researchers. This led to significant theoretical developments for prediction of elastic and inelastic constitutive response, and motivated experimental validation. The purpose of this chapter is to summarize these developments, and illustrate their application in predicting the overall response under thermomechanical loads. Although treatment of the subject in this chapter covers two-phase particulate and fibrous materials, the focus in applications will be on fibrous composites and laminates.

We begin by examining elastic composites and provide general relations among the local and overall fields. This is followed by description of two classes of models, which associate these relations with an idealized microgeometry of the composite. In one class of models, the microgeometry is not known in detail, but interaction of the phases is considered by the solution of certain inclusion problems. In the other class of models, the microstructure is idealized as a periodic dispersion of the reinforcing phase into the matrix, and a unit cell is analyzed under the applied loads. The next two sections are devoted to application of these models, when rate-independent and rate-dependent flow theories describe constitutive behavior of the phases. We close with a section on inelastic laminates where overall constitutive equations, which utilize micromechanical models of the individual plies, are developed.

The notation used here are symbolic, where symmetric second-order tensors are written as (6×1) matrices and denoted by boldface lower case letters, and symmetric fourth-order tensors are written as (6×6) matrices and denoted by boldface upper case letters. Connections with tensor notation are easily established. For example, the stress tensor, σ_{ij}, and strain tensor ε_{ij}, with the symmetry $\sigma_{ij} = \sigma_{ji}$ and $\varepsilon_{ij} = \varepsilon_{ji}$, are written in a matrix form as $\boldsymbol{\sigma} = [\sigma_{11}, \sigma_{22}, \sigma_{33}, \sigma_{23}, \sigma_{31}, \sigma_{12}]$, and $\boldsymbol{\varepsilon} = [\varepsilon_{11}, \varepsilon_{22}, \varepsilon_{33}, 2\varepsilon_{23}, 2\varepsilon_{31}, 2\varepsilon_{12}]$. Similarly, fourth-order tensors having at least the symmetries $A_{ijkl} = A_{jikl} = A_{ijlk}$ are reduced to (6×6) matrices $\mathbf{A}$, such that $\mathbf{A}\mathbf{A}^{-1} = \mathbf{A}^{-1}\mathbf{A} = \mathbf{I}$, the identity matrix.

1.14.2 MICROMECHANICS OF ELASTIC COMPOSITES

In this section, we outline the general procedure for evaluation of the local stresses and strains, as well as the overall properties of a composite medium consisting of two distinct, elastically anisotropic constituents. The constituents are assumed to be fully bonded at a defined interface, and free of voids and cracks, initially and under subsequent deformation. Loading consists of overall uniform stresses or strains as well as local transformation strains. The latter can be generated, for example, by a change of temperature or inelastic flow of the phases, and will be examined in more detail in the next two sections. In the present treatment, we assume that some localized volumes of the microstructure undergo uniform transformation strains without reference to their origin.

1.14.2.1 Governing Equations

A representative volume V of the composite aggregate is selected such that its overall response under uniform fields is identical to that of the composite. The local stresses and strains within V vary pointwise, but will be approximated by piecewise uniform fields over subvolumes V_r, $r = 1,2,\ldots Q$, such that $V = \sum V_r$, or $\sum c_r = 1$, where $c_r = V_r/V$ is the volume fraction. The number of subvolumes Q indicates the degree of refinement of the local fields. For example, a crude approximation of the local stress and strain by a piecewise uniform distribution over two subvolumes (one belongs to the matrix and the other to the fiber), provides the averaging models. On the other hand, the fiber and matrix can be subdivided into many small volumes, which reside in either phase as employed, for example, in finite element modeling of the representative volume V. Let $\boldsymbol{\sigma}_r$ and $\boldsymbol{\varepsilon}_r$ denote the average stress and strain in a subvolume such that

$$\boldsymbol{\sigma}_r = \frac{1}{V_r}\int_{V_r} \boldsymbol{\sigma}(\mathbf{x})\mathrm{d}V_r, \quad \boldsymbol{\varepsilon}_r = \frac{1}{V_r}\int_{V_r} \boldsymbol{\varepsilon}(\mathbf{x})\mathrm{d}V_r \tag{1}$$

where $\mathbf{x}$ represents the coordinates of a point in V_r. Similarly, the overall uniform stress $\boldsymbol{\sigma}$ and strain $\boldsymbol{\varepsilon}$ can be written as

$$\begin{aligned}\boldsymbol{\sigma} &= \frac{1}{V}\int_V \boldsymbol{\sigma}(\mathbf{x})\mathrm{d}V = \frac{1}{V}\sum_{r=1}^{Q}\int_{V_r} \boldsymbol{\sigma}(\mathbf{x})\mathrm{d}V_r \\ &= \sum_{r=1}^{Q} c_r\boldsymbol{\sigma}_r, \quad \boldsymbol{\varepsilon} = \sum_{r=1}^{Q} c_r\boldsymbol{\varepsilon}_r\end{aligned} \tag{2}$$

Consider elastic behavior of each homogeneous subvolume subjected to a uniform strain $\boldsymbol{\varepsilon}_r$, or stress $\boldsymbol{\sigma}_r$, and simultaneously undergoing uniform transformation strain $\boldsymbol{\mu}_r$, or stress $\boldsymbol{\lambda}_r$. In the subsequent sections, where nonlinear response is considered, we will deal with stress and strain increments rather than total quantities. Consequently, the constitutive equations of the elastic phases or subvolumes will be written in a rate form as

$$\dot{\boldsymbol{\sigma}}_r = \mathbf{L}_r\dot{\boldsymbol{\varepsilon}}_r + \dot{\boldsymbol{\lambda}}_r, \quad \dot{\boldsymbol{\varepsilon}}_r = \mathbf{M}_r\dot{\boldsymbol{\sigma}}_r + \dot{\boldsymbol{\mu}}_r \tag{3}$$

where $\mathbf{L}_r$ and $\mathbf{M}_r = \mathbf{L}_r^{-1}$ are elastic stiffness and compliance matrices. Unless there is a change of temperature, these property matrices remain constant within V_r. From Equation (3), the transformation stress and strain are related by $\boldsymbol{\lambda}_r = -\mathbf{L}_r\boldsymbol{\mu}_r$.

Similarly, the constitutive equations for the composite aggregate subjected to overall uniform strain $\boldsymbol{\varepsilon}$, or stress $\boldsymbol{\sigma}$, and undergoing uniform transformation strain $\boldsymbol{\mu}$, or stress $\boldsymbol{\lambda}$, are written as

$$\dot{\boldsymbol{\sigma}} = \mathbf{L}\dot{\boldsymbol{\varepsilon}} + \dot{\boldsymbol{\lambda}}, \quad \dot{\boldsymbol{\varepsilon}} = \mathbf{M}\dot{\boldsymbol{\sigma}} + \dot{\boldsymbol{\mu}} \tag{4}$$

where $\mathbf{L}$ and $\mathbf{M} = \mathbf{L}^{-1}$ are overall elastic stiffness and compliance matrices, and $\boldsymbol{\mu}$ and $\boldsymbol{\lambda}$ are related by $\boldsymbol{\lambda} = -\mathbf{L}\boldsymbol{\mu}$.

The connection between the overall property matrices and their local counterparts was established by Hill (1963, 1965b) in terms of phase strain and stress concentration factors, denoted respectively by $\mathbf{A}_r$ and $\mathbf{B}_r$. In the absence of transformation fields, the local strain and stress averages in the phases or subvolumes are written as

$$\dot{\boldsymbol{\varepsilon}}_r = \mathbf{A}_r\dot{\boldsymbol{\varepsilon}}, \quad \dot{\boldsymbol{\sigma}}_r = \mathbf{B}_r\dot{\boldsymbol{\sigma}} \tag{5}$$

If the concentration factors are known, one can utilize Equations (2)–(4) to find the overall elastic stiffness and compliance in the form

$$\mathbf{L} = \sum_{r=1}^{Q} c_r\mathbf{L}_r\mathbf{A}_r, \quad \mathbf{M} = \sum_{r=1}^{Q} c_r\mathbf{M}_r\mathbf{B}_r \tag{6}$$

together with the connections

$$\sum_{r=1}^{Q} c_r\mathbf{A}_r = \mathbf{I}, \quad \sum_{r=1}^{Q} c_r\mathbf{B}_r = \mathbf{I} \tag{7}$$

$$\mathbf{A}_r\mathbf{M} = \mathbf{M}_r\mathbf{B}_r, \qquad \mathbf{B}_r\mathbf{L} = \mathbf{L}_r\mathbf{A}_r \tag{8}$$

where $\mathbf{I}$ is identity matrix. When $Q = 2$, the local fields are determined as averages over the fiber and matrix phases. In this case, Equations (6) and (7) provide the concentration factors in terms of the local and overall moduli as

$$\mathbf{A}_r = (\mathbf{L}_r - \mathbf{L}_s)^{-1}(\mathbf{L} - \mathbf{L}_s)/c_r$$
$$\mathbf{B}_r = (\mathbf{M}_r - \mathbf{M}_s)^{-1}(\mathbf{M} - \mathbf{M}_s)/c_r, \quad r,s = f,m \tag{9}$$

In the presence of local transformation fields in the phases or subvolumes, V_r, $r = 1, 2, \ldots Q$, additional strains and stresses are generated and superimposed on the fields in Equation (5), to yield (Dvorak, 1992),

$$\dot{\boldsymbol{\varepsilon}}_r = \mathbf{A}_r\dot{\boldsymbol{\varepsilon}} + \sum_{r=1}^{Q} \mathbf{D}_{rs}\dot{\boldsymbol{\mu}}_s, \quad \dot{\boldsymbol{\sigma}}_r = \mathbf{B}_r\dot{\boldsymbol{\sigma}} + \sum_{r=1}^{Q} \mathbf{F}_{rs}\dot{\boldsymbol{\lambda}}_s \tag{10}$$

where $\mathbf{D}_{rs}$ and $\mathbf{F}_{rs}$, $r, s = 1, 2, \ldots Q$, are transformation influence functions. The kth column, $k = 1, 2, \ldots 6$, of $\mathbf{D}_{rs}$ evaluates the local strain $\boldsymbol{\varepsilon}_r$ in phase V_r, caused by a uniform transformation strain component μ_k of unit magnitude present in V_s under $\dot{\boldsymbol{\varepsilon}} = \mathbf{0}$. Similarly, the kth column of $\mathbf{F}_{rs}$ evaluates the local stress $\boldsymbol{\sigma}_r$ in V_r, caused by a uniform transformation stress λ_k of unit magnitude present in V_s under $\dot{\boldsymbol{\sigma}} = \mathbf{0}$.

The overall transformation stress and strain are given in terms of their local counterparts by the generalized Levin's (1967) formula (Dvorak and Benveniste, 1992),

$$\dot{\boldsymbol{\lambda}} = \sum_{r=1}^{Q} c_r\mathbf{A}_r^{\mathrm{T}}\dot{\boldsymbol{\lambda}}_r, \quad \dot{\boldsymbol{\mu}} = \sum_{r=1}^{Q} c_r\mathbf{B}_r^{\mathrm{T}}\dot{\boldsymbol{\mu}}_r \tag{11}$$

The mechanical concentration factors and the transformation influence functions depend on the micromechanical model used in approximating the local fields. In the sequel, we briefly describe two classes of models, which can be utilized to compute the concentration factors $\mathbf{A}_r$ and $\mathbf{B}_r$, and the transformation influence functions $\mathbf{D}_{rs}$ and $\mathbf{F}_{rs}$, $r, s = 1, 2, \ldots Q$, for the subvolumes V_r. Under certain approximations of the local fields, closed form expressions can be found for the influence functions in terms of the mechanical concentration factors. Considering estimates derived with the self-consistent (Hill, 1965a, 1965b or Mori and Tanaka, 1973) methods, discussed in the sequel, Dvorak and Benveniste (1992) found the following expressions for both methods,

$$\mathbf{D}_{rs} = (\mathbf{I} - \mathbf{A}_r)(\mathbf{L}_r - \mathbf{L})^{-1}(\delta_{rs}\mathbf{I} - c_s\mathbf{A}_s^{\mathrm{T}})\mathbf{L}_s \tag{12}$$

$$\mathbf{F}_{rs} = (\mathbf{I} - \mathbf{B}_r)(\mathbf{M}_r - \mathbf{M})^{-1}(\delta_{rs}\mathbf{I} - c_s\mathbf{B}_s^{\mathrm{T}})\mathbf{M}_s$$
$$r, s = 1,2,\ldots Q \tag{13}$$

with the connection

$$\mathbf{F}_{rs} = \mathbf{L}_r(\delta_{rs}\mathbf{I} - c_s\mathbf{A}_r\mathbf{B}_s^{\mathrm{T}} - \mathbf{D}_{rs})\mathbf{M}_s \tag{14}$$

where δ_{rs} is the Kronecker's tensor.

When the local fields are averaged over the fiber and matrix phases, $Q = 2$, Equations (12) and (13) reduce to (Dvorak, 1991)

$$\mathbf{D}_{rs} = (\mathbf{I}-\mathbf{A}_r)(\mathbf{L}_f-\mathbf{L}_m)^{-1}\,\mathbf{L}_s$$
$$\mathbf{F}_{rs} = (\mathbf{I}-\mathbf{B}_r)(\mathbf{M}_f-\mathbf{M}_m)^{-1}\,\mathbf{M}_s,\ r,s = f,m \qquad (15)$$

1.14.2.2 Micromechanical Models

1.14.2.2.1 Two-phase averaging models

These models utilize Eshelby's solution (Eshelby, 1957) of an ellipsoidal inhomogeneity in an infinite matrix under remotely applied uniform fields to estimate the average stresses and strains in the matrix and the fiber reinforcement. Hence, the number of subdivisions of the representative volume V in these models is $Q = 2$. Starting with the solution of a transformation problem in which a region (referred to as the inclusion), in an infinite homogeneous isotropic elastic medium undergoes a "spontaneous change of form," or eigenstrain $\boldsymbol{\mu}$, Eshelby (1957) established that if the inclusion is ellipsoidal, then the stress and strain within the inclusion are uniform, but not necessarily coaxial with $\boldsymbol{\mu}$. This important result led to the solution of several related problems. In the inhomogeneity problem, an ellipsoid of the same shape and size as the untransformed inclusion, but from a different material, is embedded in the matrix, and a uniform strain field is applied. Solution of this problem is provided by the first inclusion problem in which an "equivalent inclusion," subjected to a certain transformation strain and the given applied uniform strain field, replaces the inhomogeneity without altering the stresses or strains anywhere.

Let $\boldsymbol{\mu}$ be the unknown transformation strain to be applied to the equivalent inclusion, which has the same material properties as the surrounding matrix. The constrained uniform strain field in the inclusion is given by Eshelby (1957) as

$$\boldsymbol{\varepsilon}^C = \mathbf{S}\boldsymbol{\mu} \qquad (16)$$

where $\mathbf{S}$ is a constant matrix which depends on the shape of the ellipsoidal inclusion and Poisson's ratio of the isotropic matrix material. If a uniform strain field $\boldsymbol{\varepsilon}$ is superimposed, the strain in the inclusion is given by $(\boldsymbol{\varepsilon} + \boldsymbol{\varepsilon}^C)$, and the stress by $\mathbf{L}_1(\boldsymbol{\varepsilon} + \boldsymbol{\varepsilon}^C - \boldsymbol{\mu})$, where $\mathbf{L}_1$ is elastic stiffness of the matrix and inclusion. On the other hand, the stress in the inhomogeneity, with stiffness $\mathbf{L}_2$, is $\mathbf{L}_2\boldsymbol{\varepsilon}_2$, where $\boldsymbol{\varepsilon}_2 = \boldsymbol{\varepsilon} + \boldsymbol{\varepsilon}^C$ is the total strain. The transformation strain in the equivalent inclusion is then found by equating the stresses in the inclusion and the inhomogeneity, utilizing Equation (16),

$$\mathbf{L}_1(\boldsymbol{\varepsilon} + \mathbf{S}\boldsymbol{\mu} - \boldsymbol{\mu}) = \mathbf{L}_2\,(\boldsymbol{\varepsilon} + \mathbf{S}\boldsymbol{\mu}) \qquad (17)$$

and the strain in the inhomogeneity is found as $\boldsymbol{\varepsilon}_2 = \boldsymbol{\varepsilon}\mathbf{S}\boldsymbol{\mu}$. Alternately, $\boldsymbol{\varepsilon}_2$ can be found directly from Equations (16) and (17) after rewriting the latter as $\mathbf{L}_1(\boldsymbol{\varepsilon}_2 - \boldsymbol{\mu}) = \mathbf{L}_2\boldsymbol{\varepsilon}_2$. The result is

$$\boldsymbol{\varepsilon}_2 = [\mathbf{I} - \mathbf{S}\mathbf{L}_1^{-1}(\mathbf{L}_1 - \mathbf{L}_2)]^{-1}\boldsymbol{\varepsilon} \qquad (18)$$

This result has been utilized in several models to determine the strain and stress concentration factors in two-phase composites. Considering a dilute concentration of ellipsoids of Material 2 (the reinforcement) into a matrix of Material 1, the strain concentration factor in the reinforcement, $\mathbf{A}_2$, is given by the coefficient matrix in Equation (18) (Christensen, 1979). The corresponding stress concentration factor, $\mathbf{B}_2$, can then be found from Equation (8). Hence,

$$\mathbf{A}_2 = [\mathbf{I}-\mathbf{S}\mathbf{L}_1^{-1}\,(\mathbf{L}_1-\mathbf{L}_2)]^{-1}$$
$$\mathbf{B}_2 = \mathbf{L}_2[\mathbf{I} - \mathbf{S}\mathbf{L}_1^{-1}(\mathbf{L}_1 - \mathbf{L}_2)]^{-1}\mathbf{M} \qquad (19)$$

where $\mathbf{M}$ is the overall compliance of the composite aggregate. If the Eshelby matrix $\mathbf{S}$ is known, Equation (19) can be used to find $\mathbf{A}_2$, and Equation (7), with $Q = 2$, provides $\mathbf{A}_1$, the matrix strain concentration factor. The stress concentration factors are then found from Equations (19) and (7), where the overall compliance is given by $\mathbf{M} = \mathbf{L}^{-1}$, and the overall stiffness $\mathbf{L}$ is computed from Equation (6) with $Q = 2$.

Hill (1965b) gives a variant form of the concentration factors of Equation (19) in terms of the stiffness and compliance matrices of the cavity containing the inhomogeneity. His procedure leads to the following form of the Eshelby matrix $\mathbf{S}$

$$\mathbf{S} = \mathbf{P}\mathbf{L}_1 = \mathbf{I}-\mathbf{M}_1\mathbf{Q} \qquad (20)$$

where $\mathbf{P}$ and $\mathbf{Q}$ are related by $\mathbf{P}\mathbf{L}_1 + \mathbf{M}_1\,\mathbf{Q} = \mathbf{I}$, and depend on the shape of the ellipsoidal inclusion and elastic moduli of the matrix. In this case, the concentration factors are written as

$$\mathbf{A}_r = [\,\mathbf{I}-\mathbf{P}(\mathbf{L}_1-\mathbf{L}_r)]^{-1}$$
$$\mathbf{B}_r = [\mathbf{I}-\mathbf{Q}(\mathbf{M}_1-\mathbf{M}_r)]^{-1},\quad r = 1,2 \qquad (21)$$

We note that for the dilute approximation, where the reinforcement causes only a small perturbation of the overall field, $\mathbf{A}_1 = \mathbf{B}_1 = \mathbf{I}$. Evaluation of the concentration factors and the overall moduli is thus reduced to evaluation of

P or **Q**. Forms of **P** for various shapes of ellipsoidal inclusions can be found, for example, in Walpole (1967, 1969), Kinoshita and Mura (1971), and Mura (1982). Matrix **P** evaluated for continuous, parallel cylindrical fibers embedded in a transversely isotropic matrix is given in Section 1.14.8.

Interaction of the inhomogeneities, which is neglected in the dilute approximation, has been considered in both the self-consistent (Budiansky, 1965; Hill, 1965a, 1965b) and the Mori–Tanaka (Mori and Tanaka, 1973) methods in two different ways. In the self-consistent method, the reinforcement is embedded in a homogeneous medium, which has the effective, but yet unknown, properties of the composite. In this case, Equation (21), with $\mathbf{L}_1 = \mathbf{L}$ and $\mathbf{M}_1 = \mathbf{M}$ where **L** and **M** are overall stiffness and compliance matrices, give the concentration factors;

$$\mathbf{A}_r = [\mathbf{I}-\mathbf{P}(\mathbf{L}-\mathbf{L}_r)]^{-1}$$
$$\mathbf{B}_r = [\mathbf{I}-\mathbf{Q}(\mathbf{M}-\mathbf{M}_r)]^{-1}, \quad r = 1,2 \tag{22}$$

Since the overall properties are not known and depend on the concentration factors, Equation (22) is implicit and must be solved iteratively for the concentration factors, or the overall moduli.

The Mori–Tanaka method, on the other hand, provides explicit forms for the concentration factors. The solution is found in two steps (Benveniste, 1987). First, the reinforcement $\mathbf{L}_2$ is embedded in the matrix $\mathbf{L}_1$, and a uniform displacement field, derived from the matrix strain, is applied at the remote boundary. This provides a partial strain concentration factor, **T**, which defines the uniform strain in the reinforcement in terms of the matrix strain. An equivalent formulation can be found by subjecting the remote boundary to tractions derived from the matrix stress, and a partial stress concentration factor, **W**, is found. Using Equation (21), we find

$$\boldsymbol{\varepsilon}_2 = \mathbf{T}\boldsymbol{\varepsilon}_1, \qquad \mathbf{T} = [\mathbf{I}-\mathbf{P}(\mathbf{L}_1-\mathbf{L}_2)]^{-1} \tag{23}$$

$$\boldsymbol{\sigma}_2 = \mathbf{W}\boldsymbol{\sigma}_1, \quad \mathbf{W} = [\mathbf{I}-\mathbf{Q}(\mathbf{M}_1-\mathbf{M}_2)]^{-1} \tag{24}$$

Finally, Equation (2) is utilized to obtain the strain and stress concentration factors, for the reinforcement and the matrix, respectively, as

$$\mathbf{A}_1 = (c_1\mathbf{I} + c_2\mathbf{T})^{-1}, \quad \mathbf{A}_2 = \mathbf{T}\mathbf{A}_1 \tag{25}$$

$$\mathbf{B}_1 = (c_1\mathbf{I} + c_2\mathbf{W})^{-1}, \quad \mathbf{B}_2 = \mathbf{W}\mathbf{B}_1 \tag{26}$$

Given the concentration factors, the overall elastic stiffness and compliance matrices for two-phase composites are determined from Equation (6) with $Q = 2$. Overall elastic moduli derived from the self-consistent and Mori–Tanaka models for fibrous composites are given in Section 1.14.8.

1.14.2.2.2 Periodic array models

In this class of models, the actual material microgeometry of the composite is replaced with a certain periodic approximation. Under overall uniform fields and a uniform temperature change, the local fields possess certain symmetric features such that a unit cell can be selected for evaluation of the local fields and the overall response (Iwakuma and Nemat-Nasser, 1983; Dvorak and Teply, 1985; Teply and Dvorak, 1988; Nemat-Nasser and Hori, 1993; Walker *et al.*, 1994; Moulinec and Suquet, 1994; Buryachenko, 1996). As an application to fibrous composites, we show in Figure 1 a high contrast micrograph of the transverse plane of a boron-aluminum composite consisting of several monolayers, and its idealization by a periodic hexagonal array of fibers (Dvorak and Teply, 1985; Teply and Dvorak, 1988). Several other configurations of periodic dispersions of fibers in the transverse plane of unidirectional composites can be selected (Brockenbrough *et al.*, 1991). We note that the hexagonal fiber arrangement provides rotational symmetry about the fiber longitudinal axis, while idealizations with square and rectangular array possess only orthotropic symmetry.

In any case, a unit cell is selected and subdivided into small volumes, V_r, $r = 1, 2, \ldots Q$ such that each subvolume belongs either to the matrix or to the fiber. Evaluation of the piecewise uniform local stresses and strains in the subvolumes under overall uniform fields and uniform temperature change can proceed in two different ways. In the first approach, the overall stress and temperature time rates are applied, and the solution is found by the finite element method. The overall loading path is either known *a priori*, or derived from structural interaction of the unidirectional lamina under consideration with other plies as encountered for example in fibrous laminates (Bahei-El-Din *et al.*, 1998). Next, nodal forces that equilibrate the applied overall stresses are computed. Consider, for example, the unit cell derived from the periodic hexagonal array model (Dvorak and Teply, 1985; Teply and Dvorak, 1988) shown in Figure 2. The displacement boundary conditions consist of the six constraints indicated in Figure 2 to eliminate rigid body motions, multipoint constraints at the triangular boundary derived from the assumed

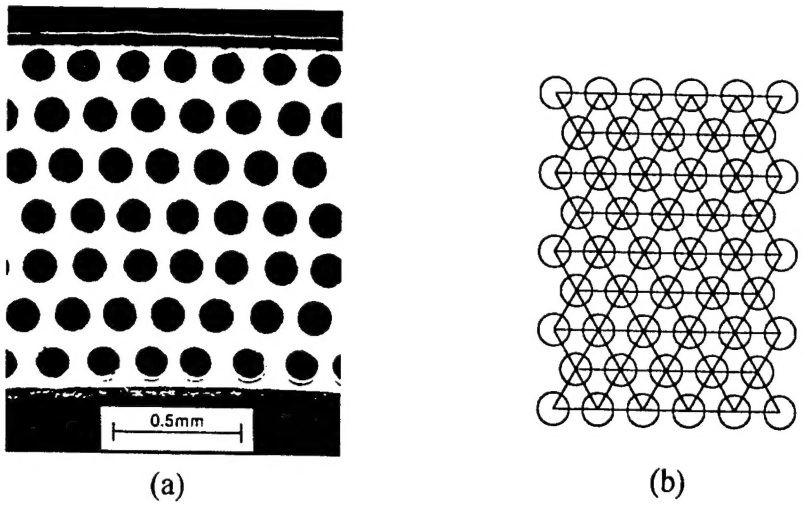

Figure 1 Transverse cross-section of a fibrous composite: (a) high contrast micrograph of a B/Al composite, $c_f = 0.45$, and (b) idealization with the periodic hexagonal array model.

periodic geometry of the microstructure, and generalized plane strain boundary conditions. Assuming a linear displacement field in an equivalent macroscopically homogeneous volume V, the method of virtual work can be used to compute the nodal forces, $\mathbf{p}_k$, $k = 1, 2, \ldots, 6$, applied at the independent degrees of freedom shown in Figure 2, from the overall stresses. The result is

$$
\begin{aligned}
p_1 &= -\frac{h}{\xi}\sigma_{22}, \quad p_2 = -\frac{h}{\xi}\sigma_{23} \\
p_3 &= -\frac{h\xi}{2}\sigma_{33} + \frac{h}{2\xi}\sigma_{23} - \frac{1}{2}\sigma_{31} \\
p_4 &= \frac{h\xi}{2}\sigma_{33} + \frac{h}{2\xi}\sigma_{23} - \frac{1}{2}\sigma_{31} \\
p_5 &= \sigma_{11}, \quad p_6 = \sigma_{12}
\end{aligned}
\tag{27}
$$

where $\xi = \sqrt[4]{3}$, and h is the length of the unit cell in the axial direction x_1, which is to be selected such that the largest aspect ratio of the finite elements is in the order of 10.

In the second approach, the unit cell is treated as an aggregate of subvolumes V_r, $r = 1, 2, \ldots, Q$, and Equation (10) is solved for the local stresses and strains. Since the local transformation fields in Equation (10) may depend on the total or incremental stress or strain, the form of the governing equations derived from Equation (10) for the local fields vary according to the underlying constitutive law of the phases. This approach, known as the transformation field analysis, has been applied by Dvorak *et al.* (1994) for viscoelastic, elastic-plastic, and viscoplastic phases, and will be described in the subsequent sections. In preparation for this solution method, the concentration factors $\mathbf{A}_r$ or $\mathbf{B}_r$, and the transformation influence functions, $\mathbf{D}_{rs}$ or $\mathbf{F}_{rs}$, $r,s = 1, 2, \ldots Q$, which depend on elastic properties of the phases and the assumed microgeometry, must be first evaluated for the selected subdivision of the unit cell.

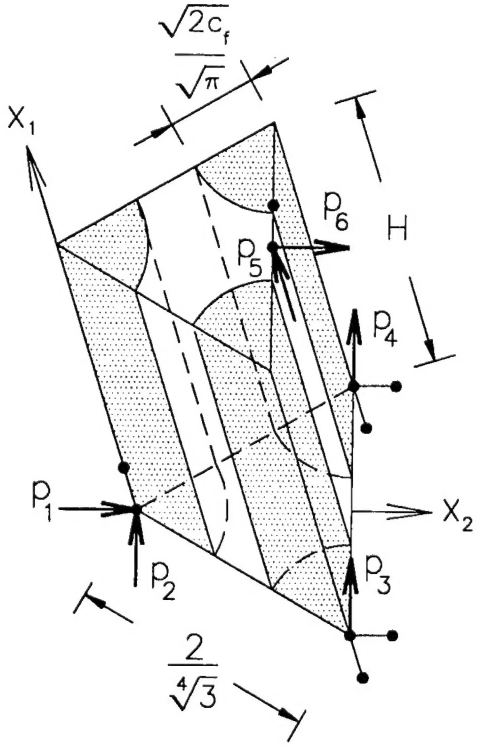

Figure 2 Geometry, constraints, and loading of the unit cell derived from the periodic hexagonal array model.

As suggested by Equation (10), the respective columns of the concentration factors $\mathbf{A}_r$ or $\mathbf{B}_r$, represent the strains, or stresses, computed in subvolume V_r under unit overall strain, or stress, components, while all subvolumes are free of transformation fields. Specifically, the kth column, $k = 1,2,\ldots, 6$, of the stress concentration matrix $\mathbf{B}_r$, $r = 1, 2,\ldots Q$, is given by the stresses caused in V_r by an overall stress component $\sigma_k = 1$. For example, the first column of $\mathbf{B}_r$ is given by the stresses caused in V_r by the overall stresses $\sigma_{11} = 1$, $\sigma_{ij} = 0$, $i,j \neq 1$. Substituting these stresses into Equation (27) provides the nodal forces

$$p_1 = p_2 = p_3 = p_4 = 0, \quad p_5 = 1, \quad p_6 = 0 \tag{28}$$

which are applied to the unit cell of Figure 2 to compute the stress concentration factors using the finite element method.

Similarly, Equation (10) suggests that the columns of the transformation matrix, $\mathbf{D}_{rs}$, $r,s = 1, 2,\ldots, Q$, represent the strains caused in subvolume V_r by unit transformation strains applied to V_s, while the unit cell is fully constrained. Specifically, if a transformation strain component $\mu_k = 1$, $k = 1, 2,\ldots, 6$, is applied to V_s, the resulting strains in subvolumes V_r, $r = 1, 2,\ldots, Q$, represent the kth column of the strain transformation factor $\mathbf{D}_{rs}$. Solution of this problem can be found by the finite element method. Let $\boldsymbol{\mu}_s$ denote the transformation strain vector applied to V_s. Using the principle of virtual work, and assuming linear variation of the displacements within each subvolume, the equivalent nodal loads are given by

$$\mathbf{p} = -V_s\overline{\mathbf{B}}^{\mathrm{T}}\mathbf{L}_s\boldsymbol{\mu}_s \tag{29}$$

where $\mathbf{L}_s$ is elastic stiffness matrix of the material in V_s and matrix $\overline{\mathbf{B}}$ relates the nodal displacements to the element strains. The local strains found in the elements of the unit cell under the nodal forces given by Equation (29) provide a column of the strain transformation matrices $\mathbf{D}_{rs}$, which corresponds to the unit transformation strain component found in $\boldsymbol{\mu}_s$. A total of $6Q$ similar problems are to be solved to compute all six columns of the transformation influence functions. However, internal symmetry of the unit cell in the transverse plane can be utilized to simplify this process (Dvorak *et al.*, 1994). Evaluation of the stress influence functions $\mathbf{F}_{rs}$ follows a similar procedure in which a unit transformation stress component $\lambda_k = 1$, $k = 1, 2,\ldots, 6$, is applied to V_s.

Under isothermal loading conditions, the concentration factors and transformation influence functions remain constant, and are computed prior to the analysis of the representative volume. On the other hand, change of the elastic moduli with temperature requires re-evaluation of all the factors in the course of the nonlinear solution. In this case, efficiency of the transformation field analysis method for periodic array models may be reduced.

1.14.3 ELASTIC-PLASTIC ANALYSIS

We now consider the solution of composite aggregates in which behavior of the phases under mechanical loads is nonlinear, but rate-independent, beyond an elastic limit or yield point. The models described above for elastic phases have been utilized in evaluation of the local stresses and strains for elastic-plastic phases. This is described in this section with results, but first a brief summary of the elastic-plastic constitutive equations of the homogeneous phases is given.

1.14.3.1 Plasticity of Homogeneous Materials

We consider a representative volume of a phase material of the composite and regard it as elastically homogeneous and isotropic on a macroscale. As usually postulated for metals, and verified by experiments, we assume the existence of a yield surface in the stress space, which is the locus of stress points that can be reached by purely elastic loading excursions from the current stress state. Furthermore, load excursions which go beyond the yield stress states cause the yield surface to distort, translate, and deform isotropically such that the current stress point is always contained by the yield surface. Neglecting distortion of the yield surface, and assuming that its isotropic deformations are caused primarily by change of the yield stress with temperature, the current yield surface can be written in the general form

$$f((\boldsymbol{\sigma}-\mathbf{a}),T) = 0 \tag{30}$$

where T is the current temperature, and $\mathbf{a}$ denotes the position of the center of the yield surface. In the absence of prior inelastic deformation, $\mathbf{a} = \mathbf{0}$, and Equation (30) defines the initial yield surface.

Assuming that plastic deformations do not affect the material symmetry found in the elastic state, specific forms of the yield function in Equation (30) are typically written in terms of stress invariants. For example, the Mises form of the yield criterion is a function of the second invariant of the stress deviation tensor, s, and is written as

$$f \equiv \frac{3}{2}(\mathbf{s} - \boldsymbol{\alpha}) : (\mathbf{s} - \boldsymbol{\alpha}) - Y^2(T) = 0 \tag{31}$$

where $\boldsymbol{\alpha}$ is the center of the yield surface in the deviatoric stress space, and Y is the yield stress in simple tension, the magnitude of which may depend on temperature. In Equation (31) we used the notation (**a**:**b**) to denote the inner product of second order tensors a_{ij} and b_{ij}.

If the strain decomposition suggested by Equation (4) into elastic and transformation parts is assumed, the stress–strain relation is written in a rate form as

$$\dot{\boldsymbol{\sigma}} = \mathbf{L}(\dot{\boldsymbol{\varepsilon}} - \dot{\boldsymbol{\varepsilon}}^p - \boldsymbol{\alpha}\dot{T}), \quad \dot{\boldsymbol{\varepsilon}} = \mathbf{M}\dot{\boldsymbol{\sigma}} + \dot{\boldsymbol{\varepsilon}}^p + \dot{\boldsymbol{\alpha}}\dot{T} \tag{32}$$

where $\boldsymbol{\alpha}$ is the coefficient of thermal expansion, and $\dot{\boldsymbol{\varepsilon}}^p$ is the plastic strain increment. The latter is a function of the current stress state and the applied stress increment. Whether or not a plastic strain increment will develop when a stress increment is applied from a current state, which satisfies the yield function depends on the loading direction. Under thermomechanical load increments, the possible states found under loading from the current yield surface are:

$$\dot{\boldsymbol{\varepsilon}}^p = \mathbf{0} \text{ for } f = 0, \quad \left(\frac{\partial f}{\partial \boldsymbol{\sigma}}\right) : \dot{\boldsymbol{\sigma}} + \frac{\partial f}{\partial T}\dot{T} < 0 \tag{33}$$

$\Rightarrow$ elastic state or unloading

$$\dot{\boldsymbol{\varepsilon}}^p = \mathbf{0} \text{ for } f = 0, \quad \left(\frac{\partial f}{\partial \boldsymbol{\sigma}}\right) : \dot{\boldsymbol{\sigma}} + \frac{\partial f}{\partial T}\dot{T} = 0 \tag{34}$$

$\Rightarrow$ neutral loading

$$\dot{\boldsymbol{\varepsilon}}^p \neq \mathbf{0} \text{ for } f = 0, \quad \left(\frac{\partial f}{\partial \boldsymbol{\sigma}}\right) : \dot{\boldsymbol{\sigma}} + \frac{\partial f}{\partial T}\dot{T} > 0 \tag{35}$$

$\Rightarrow$ plastic loading

Stress states which fall outside the elastic domain bounded by the yield surface in Equations (30) or (31) are not allowed. Consequently, the yield surface expands isotropically and/or translates to contain the stress points that satisfy Equation (35). Any hardening rule postulated for the yield surface must conform to Prager's (1955) consistency condition

$$\dot{f} \equiv \left(\frac{\partial f}{\partial \boldsymbol{\sigma}}\right) : (\dot{\boldsymbol{\sigma}} - \underline{\mathbf{a}}) + \frac{\partial f}{\partial T}\dot{T} = 0 \tag{36}$$

written here for kinematic hardening, while isotropic changes in the yield surface are caused by change of the yield surface with temperature. Evolution laws for the center of the yield surface **a** were suggested early on by Prager (1955) and modified by Ziegler (1959). More recent experiments conducted by Phillips and co-workers (Phillips *et al.*, 1972; Phillips and Moon, 1977; Phillips and Lee, 1979) on commercial aluminum, and by Dvorak *et al.* (1988) on 6061 aluminum, indicated that the yield surface translates in the direction of the applied stress increment to accommodate the stress point. The magnitude of the translation, however, must be adjusted if the yield stress varies with temperature. Under thermomechanical loading, the Phillips law is written as (Bahei-El-Din, 1990)

$$\dot{\mathbf{a}} = \gamma\dot{\boldsymbol{\sigma}} \tag{37}$$

and the scalar γ is found by satisfying the consistency condition in Equation (36). For the Mises yield surface in Equation (31), the result is

$$\gamma = 1 - \frac{Y(T)Y'(T)\dot{T}}{\frac{3}{2}(\mathbf{s} - \boldsymbol{\alpha}) : \dot{\boldsymbol{\sigma}}} \tag{38}$$

where $Y'(T) = \mathrm{d}Y/\mathrm{d}T$.

The direction of the plastic strain increment is established with the normality rule, a consequence of Drucker's (1952) postulate for a stable material,

$$\dot{\boldsymbol{\varepsilon}}^p = \dot{\Gamma}\frac{\partial f}{\partial \mathbf{s}} \tag{39}$$

The magnitude of the scalar $\dot{\Gamma}$ is evaluated from Ziegler's (1959) equality,

$$c\dot{\boldsymbol{\varepsilon}}^p : \frac{\partial f}{\partial \mathbf{s}} = \underline{\mathbf{a}} : \frac{\partial f}{\partial \mathbf{s}} \tag{40}$$

For the Mises yield surface in Equation (31), Equations (39) and (40) give

$$\dot{\boldsymbol{\varepsilon}}^p = \left(\frac{3}{2H(T)}(\mathbf{n}^{\mathrm{T}}.\dot{\boldsymbol{\sigma}}) - \sqrt{\tfrac{3}{2}}\frac{Y'(T)}{H(T)}\dot{T}\right)\mathbf{n} \tag{41}$$

where $H(T)$ is plastic tangent modulus of the stress–plastic strain curve, determined from a simple tension test, and defined for multidimensional stress state as

$$H(T) = \frac{(\dot{\bar{\sigma}} - Y'(T)\dot{T})}{\dot{\bar{\varepsilon}}^p}, \quad \dot{\bar{\sigma}} = \left(\tfrac{3}{2}\dot{\mathbf{s}} : \dot{\mathbf{s}}\right)^{\frac{1}{2}}$$
$$\dot{\bar{\varepsilon}}^p = \left(\tfrac{2}{3}\dot{\boldsymbol{\varepsilon}}^p : \dot{\boldsymbol{\varepsilon}}^p\right)^{\frac{1}{2}} \tag{42}$$

and **n** is the unit normal to the yield surface at the current stress point. For the Mises yield surface in Equation (31), **n** is given by

$$\mathbf{n} = \frac{1}{\sqrt{\tfrac{2}{3}}Y}\left[\hat{s}_{11} \quad \hat{s}_{22} \quad \hat{s}_{33} \quad 2\hat{s}_{23} \quad 2\hat{s}_{31} \quad 2\hat{s}_{12}\right]^{\mathrm{T}}$$
$$\hat{\mathbf{s}} = \mathbf{s} - \boldsymbol{\alpha} \tag{43}$$

The constitutive law described above can now be cast in one of two forms to be utilized

in the micromechanical models of Section 1.14.2.2. In the first form, the stress–strain relations are written in terms of instantaneous moduli. Hence, for thermomechanical loading, we write

$$\dot{\boldsymbol{\sigma}} = \boldsymbol{\mathcal{L}}\dot{\boldsymbol{\varepsilon}} + \boldsymbol{\ell}\dot{T}, \dot{\boldsymbol{\varepsilon}} = \boldsymbol{\mathcal{M}}\dot{\boldsymbol{\sigma}} + \boldsymbol{m}\dot{T} \tag{44}$$

where $\boldsymbol{\mathcal{L}}$ and $\boldsymbol{\mathcal{M}}$ are instantaneous, elastic-plastic stiffness and compliance matrices, and $\boldsymbol{\ell}$ and $\boldsymbol{m}$ are instantaneous thermal stress and strain vectors. Assuming additive decomposition of elastic and inelastic strains, these property matrices can be written from the constitutive equations described above, for a Mises yield surface, as (Bahei-El-Din, 1990)

$$\boldsymbol{\mathcal{L}} = \mathbf{L} + \boldsymbol{\mathcal{L}}^p = \boldsymbol{\mathcal{M}}^{-1}, \quad \boldsymbol{\mathcal{M}} = \mathbf{M} + \boldsymbol{\mathcal{M}}^p \tag{45}$$

$$\boldsymbol{\mathcal{L}}^p = -\left(\frac{2G}{1 + H/3G}\right)[\mathbf{n}.\mathbf{n}^{\mathrm{T}}], \quad \boldsymbol{\mathcal{M}}^p = \left(\frac{3}{2H}\right)[\mathbf{n}.\mathbf{n}^{\mathrm{T}}] \tag{46}$$

$$\boldsymbol{\ell} = \mathbf{l} + \boldsymbol{\ell}^p = -\boldsymbol{\mathcal{L}}\,\boldsymbol{m}, \quad \boldsymbol{m} = \boldsymbol{\alpha} + \boldsymbol{m}^p \tag{47}$$

$$\mathbf{l} = -\mathbf{L}\boldsymbol{\alpha}, \boldsymbol{\ell}^p = \left(\frac{2G}{1 + H/3G}\right)\left(\mathbf{n}^{\mathrm{T}}.\boldsymbol{\alpha} + \frac{Y'(T)}{\sqrt{6}G}\right)\mathbf{n}$$
$$\boldsymbol{m}^p = -\left(\sqrt{\tfrac{3}{2}}\frac{Y'(T)}{H}\right)\mathbf{n} \tag{48}$$

where G is elastic shear modulus.

Alternately, the stress–strain equations can be written in the equivalent form suggested in Equation (4),

$$\dot{\boldsymbol{\sigma}} = \mathbf{L}\dot{\boldsymbol{\varepsilon}} + \dot{\boldsymbol{\lambda}}, \quad \dot{\boldsymbol{\varepsilon}} = \mathbf{M}\dot{\boldsymbol{\sigma}} + \dot{\boldsymbol{\mu}} \tag{49}$$

where

$$\mathbf{L} = \mathbf{M}^{-1}, \quad \dot{\boldsymbol{\lambda}} = -\mathbf{L}\dot{\boldsymbol{\mu}}, \tag{50}$$

$$\dot{\boldsymbol{\mu}} = \dot{\boldsymbol{\varepsilon}} - \dot{\boldsymbol{\varepsilon}}^{\mathrm{e}} = \boldsymbol{\mathcal{M}}^{\mathrm{p}}\dot{\boldsymbol{\sigma}} + (\boldsymbol{\alpha} + \boldsymbol{m}^{\mathrm{p}})\dot{T} \tag{51}$$

For a Mises yield criterion, Equation (51) provides

$$\dot{\boldsymbol{\mu}} = \left(\frac{3}{2H}(\mathbf{n}^{\mathrm{T}}.\dot{\boldsymbol{\sigma}}) - \sqrt{\tfrac{3}{2}}\frac{Y'(T)}{H}\dot{T}\right)\mathbf{n} + \boldsymbol{\alpha}\dot{T} \tag{52}$$

1.14.3.2 Plasticity of Composite Materials

The micromechanical models of elasticity described in Section 1.14.2 can now be combined with the phase constitutive equations of plasticity to compute the overall response and local stress and strain fields in composite materials. The method depends on the micromechanical model used. First, consider two phase averaging models, Section 1.14.2.2.1, and assume that both the fiber and matrix phases are elastic-plastic with instantaneous properties given by Equations (45)–(48). In analogy with Equations (5)–(9), stress and strain increments in the phases can be written for mechanical loading as

$$\dot{\boldsymbol{\varepsilon}}_r = \boldsymbol{\mathcal{A}}_r\dot{\boldsymbol{\varepsilon}}, \quad \dot{\boldsymbol{\sigma}}_r = \boldsymbol{\mathcal{B}}_r\dot{\boldsymbol{\sigma}}, \quad r = f,m \tag{53}$$

where $\boldsymbol{\mathcal{A}}_r$ and $\boldsymbol{\mathcal{B}}_r$ are instantaneous strain and stress concentration factors, given by

$$\boldsymbol{\mathcal{A}}_r = (\boldsymbol{\mathcal{L}}_r - \boldsymbol{\mathcal{L}}_s)^{-1}(\boldsymbol{\mathcal{L}} - \boldsymbol{\mathcal{L}}_s)/c_r$$
$$\boldsymbol{\mathcal{B}}_r = (\boldsymbol{\mathcal{M}}_r - \boldsymbol{\mathcal{M}}_s)^{-1}(\boldsymbol{\mathcal{M}} - \boldsymbol{\mathcal{M}}_s)/c_r, \quad r,s = f,m \tag{54}$$

The overall instantaneous stiffness and compliance matrices $\boldsymbol{\mathcal{L}}$ and $\boldsymbol{\mathcal{M}}$ are given by

$$\boldsymbol{\mathcal{L}} = c_f\boldsymbol{\mathcal{L}}_f\boldsymbol{\mathcal{A}}_f + c_m\boldsymbol{\mathcal{L}}_m\boldsymbol{\mathcal{A}}_m$$
$$\boldsymbol{\mathcal{M}} = c_f\boldsymbol{\mathcal{M}}_f\boldsymbol{\mathcal{B}}_f + c_m\boldsymbol{\mathcal{M}}_m\boldsymbol{\mathcal{B}}_m \tag{55}$$

Since the response of the material is a function of the past loading history, the instantaneous moduli are not known *a priori*, and the concentration factors cannot be evaluated from Equation (54). Instead, averaging models derived in Section 1.14.2.2.1 for elastic phases are used to compute the concentration factors, after replacing the phase elastic properties by the instantaneous moduli. We recall that the averaging models described in Section 1.14.2.2.1 represent various interpretations of the concentration factors given in Equation (19), which was derived from Eshelby's equivalent inclusion problem. When the matrix instantaneous properties are used to solve the elastic-plastic problem, we are effectively solving successive problems of the Eshelby type assuming that the matrix is elastically anisotropic. In this case, evaluation of the Eshelby matrix $\mathbf{S}$ can be performed only numerically (Ghahremani, 1977).

The above approach has been widely implemented for both isothermal and thermomechanical loads (see, for example, Bahei-El-Din, 1990 and Lagoudas *et al.*, 1991). The method however is known to produce overall and phase strain predictions that violate the rigorous Levin's formula in Equation (11). The source of this violation and related inaccuracies of the predictions are traced to application of the plasticity constitutive law using phase average stresses. A more refined approximation of the local fields is desired when the constitutive behavior of the phases deviates from linearity. This is offered by the transformation field analysis (Dvorak *et al.*, 1994).

The method centers on Equation (10) which evaluates the local fields as the sum of contri-

butions from the overall fields applied to an elastic aggregate, and the local transformation fields. If the latter are caused by thermoplastic deformation of the phases, Equation (51) is applied to each subvolume to obtain the increment of transformation strain corresponding to the current stress state and temperature. Substituting Equation (51) into Equation (10), we find

$$\dot{\boldsymbol{\sigma}}_r = \mathbf{B}_r\dot{\boldsymbol{\sigma}} - \sum_{s=1}^{Q}\mathbf{F}_{rs}\mathbf{L}_s\left(\boldsymbol{\mathcal{M}}_s^p\dot{\boldsymbol{\sigma}}_s + (\boldsymbol{\alpha}_s + \boldsymbol{m}_s^p)\dot{T}\right) \tag{56}$$

From Equation (56), the array of local stress increments $\{\dot{\boldsymbol{\sigma}}_r\} = \{\dot{\boldsymbol{\sigma}}_1, \dot{\boldsymbol{\sigma}}_2, \ldots \dot{\boldsymbol{\sigma}}_Q\}$ can be written as

$$\{\dot{\boldsymbol{\sigma}}_r\} = [\mathrm{diag}(\mathbf{I}) + [\mathbf{F}_{rs}\mathbf{L}_s\boldsymbol{\mathcal{M}}_s^p]]^{-1}$$
$$\{[\mathbf{B}_r]\dot{\boldsymbol{\sigma}} - [\mathbf{F}_{rs}\,\mathbf{L}_s]\{\boldsymbol{\alpha}_s + \boldsymbol{m}_s^p\}\,\dot{T}\} \tag{57}$$

Equation (57) is written for a Mises material as

$$\{\dot{\boldsymbol{\sigma}}_r\} = \left[\mathrm{diag}(\mathbf{I}) + \tfrac{3}{2}\left[\frac{1}{H_s}\mathbf{F}_{rs}\mathbf{L}_s\mathbf{n}_s\mathbf{n}_s^{\mathrm{T}}\right]\right]^{-1}$$
$$\left\{[\mathbf{B}_r]\dot{\boldsymbol{\sigma}} - [\mathbf{F}_{rs}\mathbf{L}_s]\left\{\boldsymbol{\alpha}_s - \sqrt{\tfrac{3}{2}}\frac{Y_s'(T)}{H_s}\mathbf{n}_s\right\}\dot{T}\right\} \tag{58}$$

Integration of Equation (58) along the loading path $(\dot{\boldsymbol{\sigma}}, \dot{T})$ provides the local stresses. The local strain increments are found from Equation (44), and the overall inelastic strain increments from the generalized Levin's formula in Equation (11).

For a Mises yield criterion, the transformation strains in the subvolumes are given by Equation (52). In this case, Equation (11) provides

$$\dot{\boldsymbol{\mu}} = \dot{\boldsymbol{\varepsilon}}^p + \boldsymbol{\alpha}\dot{T} \tag{59}$$

$$\dot{\boldsymbol{\varepsilon}}^p = \sum_{r=1}^{Q} c_r\left(\frac{3}{2H_r}\mathbf{n}_r^{\mathrm{T}}\dot{\boldsymbol{\sigma}}_r - \sqrt{\tfrac{3}{2}}\frac{Y_r'(T)}{H_r}\dot{T}\right)\mathbf{B}_r^{\mathrm{T}}\mathbf{n}_r \tag{60}$$

$$\boldsymbol{\alpha} = \sum_{r=1}^{Q} c_r\mathbf{B}_r^{\mathrm{T}}\boldsymbol{\alpha}_r \tag{61}$$

where $\dot{\boldsymbol{\varepsilon}}^p$ is the overall plastic strain increment, and $\boldsymbol{\alpha}$ is the overall coefficient of thermal expansion.

Equation (57) can be used to derive overall instantaneous property matrices and thermal strains which can be utilized in finite element analysis of composite structures in which the elements are treated as macroscopically homogeneous with properties derived from a micromechanical model (Bahei-El-Din *et al.*, 1981). Comparing Equation (57) with Equation (53), the instantaneous stress concentration factors in subvolume V_r, $r = 1,2,\ldots Q$, are written as

$$[\boldsymbol{\mathcal{B}}_r] = [\mathrm{diag}(\mathbf{I}) + [\mathbf{F}_{rs}\mathbf{L}_s\boldsymbol{\mathcal{M}}_s^p]]^{-1}\,[\mathbf{B}_r] \tag{62}$$

The overall instantaneous compliance is then found as

$$\boldsymbol{\mathcal{M}} = \sum_{r=1}^{Q} c_r\boldsymbol{\mathcal{M}}_r\boldsymbol{\mathcal{B}}_r$$
$$= \sum_{r=1}^{Q} c_r\boldsymbol{\mathcal{M}}_r\left[\mathrm{diag}(\mathbf{I}) + \left[\mathbf{F}_{rs}\mathbf{L}_s\boldsymbol{\mathcal{M}}_s^p\right]\right]^{-1}[\boldsymbol{\mathcal{B}}_r] \tag{63}$$

A similar procedure leads to

$$[\boldsymbol{\mathcal{A}}_r] = [\mathrm{diag}(\mathbf{I}) + [\mathbf{D}_{rs}\boldsymbol{\mathcal{M}}_s\boldsymbol{\mathcal{L}}_s^p]]^{-1}[\mathbf{A}_r], \tag{64}$$

$$\boldsymbol{\mathcal{L}} = \sum_{r=1}^{Q} c_r\boldsymbol{\mathcal{L}}_r\boldsymbol{\mathcal{A}}_r$$
$$= \sum_{r=1}^{Q} c_r\boldsymbol{\mathcal{L}}_r\left[\mathrm{diag}(\mathbf{I}) + \left[\mathbf{D}_{rs}\mathbf{M}_s\boldsymbol{\mathcal{L}}_s^p\right]\right]^{-1}[\mathbf{A}_r] \tag{65}$$

where $\boldsymbol{\mathcal{A}}_r$ is the instantaneous strain concentration factor in V_r, and $\boldsymbol{\mathcal{L}}$ is the overall instantaneous stiffness matrix. The overall thermal strain is found from Equations (11) and (47) as

$$\boldsymbol{m} = \sum_{r=1}^{Q} c_r\boldsymbol{\mathcal{B}}_r^{\mathrm{T}}\left(\boldsymbol{\alpha}_r + \boldsymbol{m}_r^p\right) \tag{66}$$

For a Mises yield criterion, Equations (62)–(66) provide

$$[\boldsymbol{\mathcal{A}}_r] = \left[\mathrm{diag}(\mathbf{I}) - \left[\left(\frac{2G_s}{1 + H_s/3G_s}\right)\mathbf{D}_{rs}\mathbf{M}_s\left[\mathbf{n}_s\mathbf{n}_s^{\mathrm{T}}\right]\right]\right]^{-1}$$
$$[\mathbf{A}_r] \tag{67}$$

$$[\boldsymbol{\mathcal{B}}_r] = \left[\mathrm{diag}(\mathbf{I}) + \tfrac{3}{2}\left[\frac{1}{H_s}\mathbf{F}_{rs}\mathbf{L}_s\mathbf{n}_s\mathbf{n}_s^{\mathrm{T}}\right]\right]^{-1}[\mathbf{B}_r] \tag{68}$$

$$\boldsymbol{\mathcal{L}} = \sum_{r=1}^{Q} c_r\boldsymbol{\mathcal{L}}_r$$
$$\left[\mathrm{diag}(\mathbf{I}) - \left(\frac{2G_s}{1 + H_s/3G_s}\right)\left[\mathbf{D}_{rs}\mathbf{M}_s\left[\mathbf{n}_s\mathbf{n}_s^{\mathrm{T}}\right]\right]\right]^{-1}[\mathbf{A}_r], \tag{69}$$

$$\boldsymbol{\mathcal{M}} = \sum_{r=1}^{Q} c_r\boldsymbol{\mathcal{M}}_r\left[\mathrm{diag}(\mathbf{I}) + \tfrac{3}{2}\left[\frac{1}{H_s}\mathbf{F}_{rs}\mathbf{L}_s\mathbf{n}_s\mathbf{n}_s^{\mathrm{T}}\right]\right]^{-1}[\mathbf{B}_r] \tag{70}$$

$$\boldsymbol{m} = \sum_{r=1}^{Q} c_r\mathbf{B}_r^{\mathrm{T}}\left(\boldsymbol{\alpha}_r - \sqrt{\tfrac{3}{2}}\frac{Y_r'(T)\dot{T}}{H_r}\mathbf{n}_r\right) \tag{71}$$

1.14.3.3 Bimodal Plasticity of Fibrous Composites

The micromechanical models discussed above for elastic-plastic phases provide the overall instantaneous strains as well as the local fields, but can also be used to find the overall yield surface. Consider, for example, a two-phase composite in which the fiber is elastic and the matrix is elastic-plastic with a yield criterion described by the Mises yield surface (31). Let $\boldsymbol{s}_m$ and $\boldsymbol{a}_m$ denote the matrix deviatoric stress and center of the yield surface, respectively. If $\boldsymbol{s}$ and $\boldsymbol{a}$ denote their overall counterparts, and since both the vectors $(\boldsymbol{s}_m - \boldsymbol{a}_m)$ and $(\boldsymbol{s} - \boldsymbol{a})$ fall inside their respective yield surfaces, we can write

$$(\boldsymbol{s}_m - \boldsymbol{a}_m) = \mathbf{B}_m(\boldsymbol{s} - \boldsymbol{a}) \tag{72}$$

where $\mathbf{B}_m$ is the matrix stress concentration factor. Substituting Equation (72) into Equation (31), after the latter is rewritten with index m to denote matrix-related variables, the overall yield surface is found in the deviatoric stress space as

$$f \equiv \frac{3}{2}[\mathbf{B}_m(\boldsymbol{s} - \boldsymbol{a})] : [\mathbf{B}_m(\boldsymbol{s} - \boldsymbol{a})] - Y_m^2(T) = 0 \tag{73}$$

In the overall stress space $\boldsymbol{\sigma}$, the yield surface in Equation (73) is given by

$$f \equiv (\boldsymbol{\sigma} - \mathbf{a})^{\mathrm{T}}(\mathbf{B}_m^{\mathrm{T}}\mathbf{C}\mathbf{B}_m)(\boldsymbol{\sigma} - \mathbf{a}) - Y_m^2(T) = 0 \tag{74}$$

where $\mathbf{a}$ is the center of the overall yield surface, and $\mathbf{C}$ is a symmetric 6×6 matrix with the following nonzero coefficients, $C_{11} = C_{22} = C_{33} = 1$, $C_{12} = C_{13} = C_{23} = -1/2$, $C_{44} = C_{55} = C_{66} = 3$. Overall stress excursions which fall in the stress domain enclosed by the ellipsoidal yield surface in Equation (74) cause only elastic deformation of the matrix. Dimensions of the overall yield surface depend on magnitude of the matrix yield stress, and the volume fraction of the fiber and matrix as well as their elastic moduli.

Motivated by experimental results, the bimodal plasticity theory (Dvorak and Bahei-El-Din, 1987) postulates that yielding of the matrix according to the criterion given by Equation (73) takes place in fibrous systems only under loading conditions which allow both the fiber and matrix to participate in carrying the applied load. Hence, this deformation mode is referred to as the fiber-dominated mode (FDM). On the other hand, the matrix-dominated mode (MDM) assumes that the applied load is carried by the matrix, while the fiber constrains the matrix plastic deformation to simple shear straining on planes that are parallel to the fiber longitudinal axis. The matrix-dominated mode is thus represented by a variant of the continuum slip-model.

The initial yield condition on any potential slip plane (k) is taken as,

$$f\left(\tau^{(k)}\right) = \left(\max \tau_{ns}^{(k)}\right)^2 - \tau_o^2 = 0 \tag{75}$$

where τ_{ns} denotes the resolved shear stress, and τ_o is the matrix yield stress in simple shear. The active slip system is defined by the normal n_i to the slip plane, and by the slip direction s_j, so that the resolved shear stress is

$$\tau_{ns}^{(k)} = n_i^{(k)}\sigma_{ij}s_j^{(k)} = \left(\tau_1^2 + \tau_2^2\right)_k^{1/2} \tag{76}$$

Considering plane stresses in the x_1x_2-plane (Figure 3), where the x_1-axis is parallel to the fiber longitudinal axis, the components τ_1 and τ_2 of the resolved shear stress τ_{ns} are given by

$$\tau_1 = \sigma_{21}\cos\beta, \quad \tau_2 = \frac{1}{2}\sigma_{22}\sin 2\beta \tag{77}$$

The maximum resolved shear stress is evaluated from

$$\tau_{ns}\left(\frac{\partial \tau_{ns}}{\partial \beta}\right) = \tau_1\left(\frac{\partial \tau_1}{\partial \beta}\right) + \tau_2\left(\frac{\partial \tau_2}{\partial \beta}\right) = 0 \tag{78}$$

For the slip system on the plane $k = 1$, Equations (76)–(78) provide

$$\beta_1 = \frac{1}{2}\cos^{-1}q^2 \text{ for } |q| \leqslant 1, \quad \beta_1 = 0 \text{ for } |q| \geqslant 1 \tag{79}$$

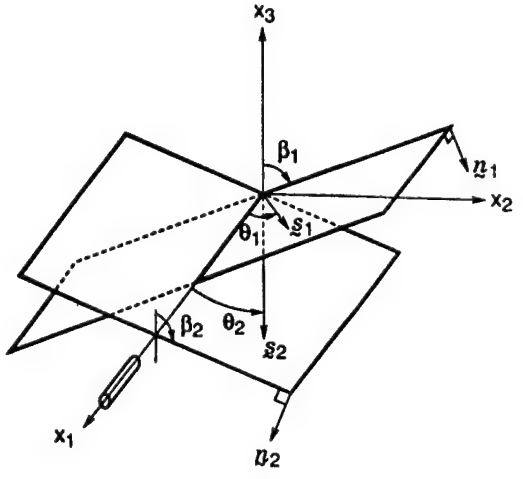

Figure 3 Geometry of the conjugate slip systems of the matrix-dominated deformation mode.

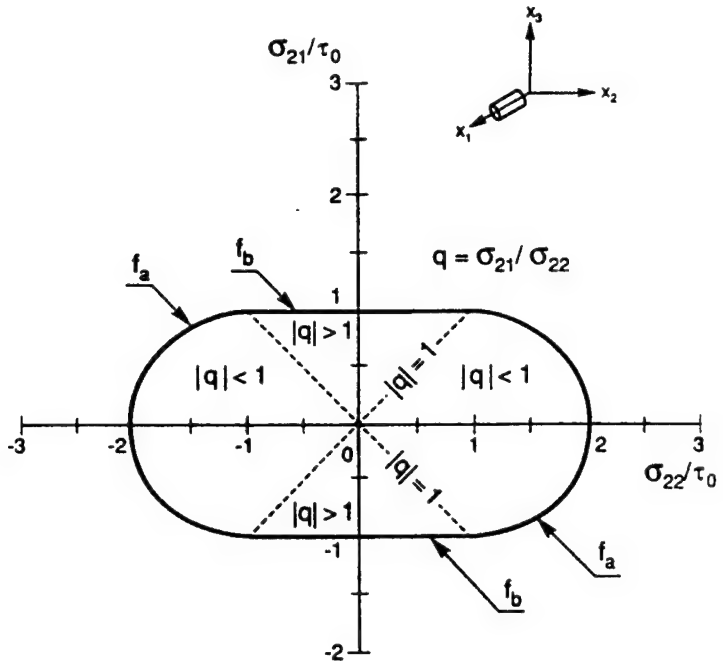

Figure 4 Transverse cross-section of the initial yield surface of the matrix-dominated deformation mode.

where $q = \sigma_{21}/\sigma_{22}$ if $\sigma_{22} \neq 0$, and the angle θ_1 between the slip direction and the x_1-axis is given by

$$\tan \theta_1 = \frac{1}{q} \sin \beta_1 \tag{80}$$

The conjugate system on the plane $k = 2$ in Figure 3 is specified by the angles β_2 and θ_2 that are related to β_1 and θ_1 by

$$\begin{aligned} &\beta_2 = \pi - \beta_1, \theta_2 = \theta_1 \text{ for } |q| \leqslant 1 \\ &\beta_2 = 0, \theta_2 = \theta_1 \text{ for } |q| \geqslant 1 \end{aligned} \tag{81}$$

where $0 \leqslant \beta_1 \leqslant \pi/4$ and $0 \leqslant \theta_1 \leqslant 2\pi$.

Substituting the slip system parameters that assure maxima of the resolved shear stress under the applied overall plane stress state, and assuming kinematic hardening for the matrix, one finds the overall MDM yield condition as

$$\begin{aligned} f_a &= \left(\frac{\sigma_{21} - a_{21}}{\tau_o}\right)^2 \\ &\quad + \left(\frac{\sigma_{22} - a_{22}}{\tau_o} \mp 1\right)^2 - 1 = 0 \text{ for } |q| \leqslant 1 \\ f_b &= \left(\frac{\sigma_{21} - a_{21}}{\tau_o}\right)^2 - 1 = 0 \text{ for } |q| \geqslant 1 \end{aligned} \tag{82}$$

These relations suggest that the MDM yield surface in the overall plane stress space is an open cylinder with oval cross-section in the $\sigma_{22}\sigma_{21}$-plane, and generators parallel to the σ_{11}-axis. The cross-section of the MDM yield cylinder for the initial state $a_{11} = a_{22} = 0$, is shown in Figure 4. Note that this surface is independent of phase moduli and volume fractions.

The overall yield surface is given by the internal envelope of the FDM yield surface in Equation (74), projected into the σ_{11}, σ_{22}, σ_{21} stress space, and the MDM yield surface branch in Equation (82). The experimental results that follow show that the shape and position of the observed yield surfaces are closely predicted by the bimodal theory combined with the Phillips kinematic hardening rule (Equations (37) and (38)).

1.14.3.4 Experimental Results and Predictions

In this section, we present a sample of the experimental results obtained in an extensive study of the behavior of boron-aluminum fibrous systems (Dvorak *et al.*, 1988; Nigam *et al.*, 1994a, 1994b), together with predictions using the methods outlines in Sections 1.14.3.2 and 1.14.3.3. The experiments were conducted on thin-walled tube specimens fabricated by diffusion bonding of seven monolayer 6061-Al/B sheets. The fibers were aligned parallel to the meridians of the tube, at a volume fraction $c_f = 0.45$. Figure 5 shows the geometry and instrumentation of the tube. A cross-section of the tube is shown in Figure 1(a).

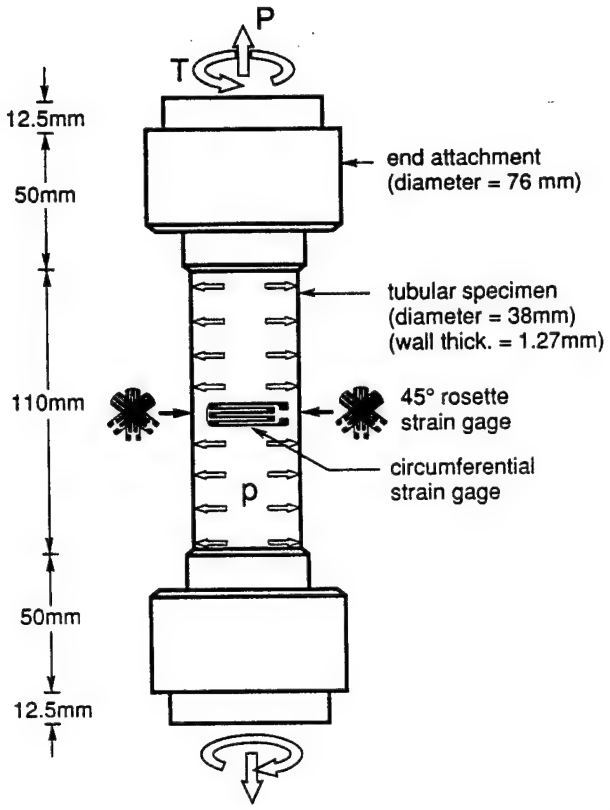

Figure 5 Dimensions and instrumentation of the composite tube specimen.

The specimens were loaded by axial force, internal pressure, and torsion, applied according to various routines. Here we consider a specific loading regime in which the specimen was subjected to internal pressure and torque. This produced transverse normal stress σ_{22}, longitudinal shear stress σ_{21} and axial normal stress $\sigma_{11} = \frac{1}{2}\sigma_{22}$. The axial stress was caused by the internal pressure, and was not compensated for in the experiment. Consequently, this loading regime can be represented in a stress plane consisting of the shear stress σ_{21} and the resultant normal stress $\sqrt{\sigma_{11}^2 + \sigma_{22}^2} = \frac{\sqrt{5}}{2}\sigma_{22}$. This is shown in Figure 6, where the loading path is indicated by the diamond symbols, labeled 0, 1, ..., 11.

The overall initial yield surface and three subsequent surfaces that were detected in the experiment are shown in Figure 6. The loading path followed before evaluation of the subsequent yield surfaces is indicated in the Figure. At each point on the yield surface, the yield stress was defined by back extrapolation from a small excursion into the plastic region, at zero offset strain. The experimental yield surfaces were constructed by fitting the appropriate sections of the bimodal yield surfaces, Equations (74) and (82). Apart from the change in the size of the yield surfaces, the bimodal theory predicts quite closely the shape of the overall yield surface in the loading plane of this experiment. Similar agreement between the yield surfaces detected experimentally and those evaluated with the bimodal theory was found under several other loading regimes (Nigam *et al.*, 1994a, 1994b).

Figures 7–9 show the comparisons between the predictions of plastic strains along the path of Figure 6. The predictions were obtained from the periodic hexagonal array (PHA) model with two different meshes, the matrix mode of the bimodal theory, and the Mori–Tanaka model. The matrix constitutive equations described in Section 1.14.3.1 were used in all models. The comparisons indicate that both the Mori–Tanaka and bimodal theories, which compute the plastic strain using the matrix stress average, fail to approximate the actual plastic strains. In contrast, the PHA model provides a reasonable approximation, even with a small number of element subdivisions.

1.14.4 VISCOPLASTIC ANALYSIS

In this section, we describe solution of the composite aggregate when the rate of loading

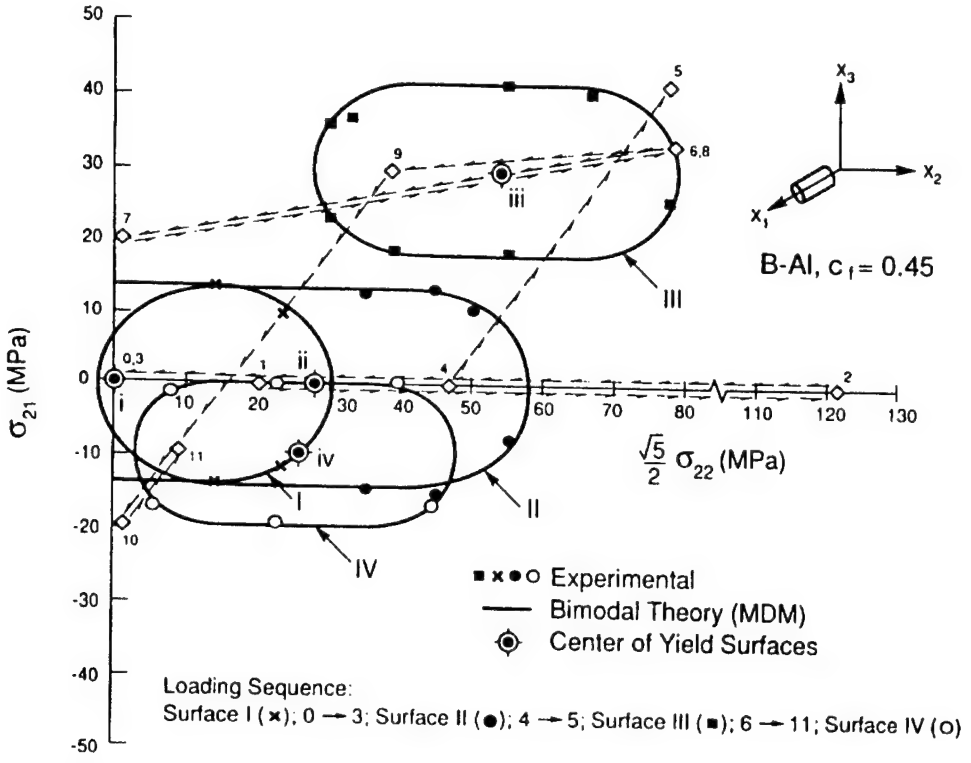

Figure 6 Loading path applied to the B/Al composite tube in the transverse tension-longitudinal shear stress space, with experimental yield points and matrix-dominated yield surfaces.

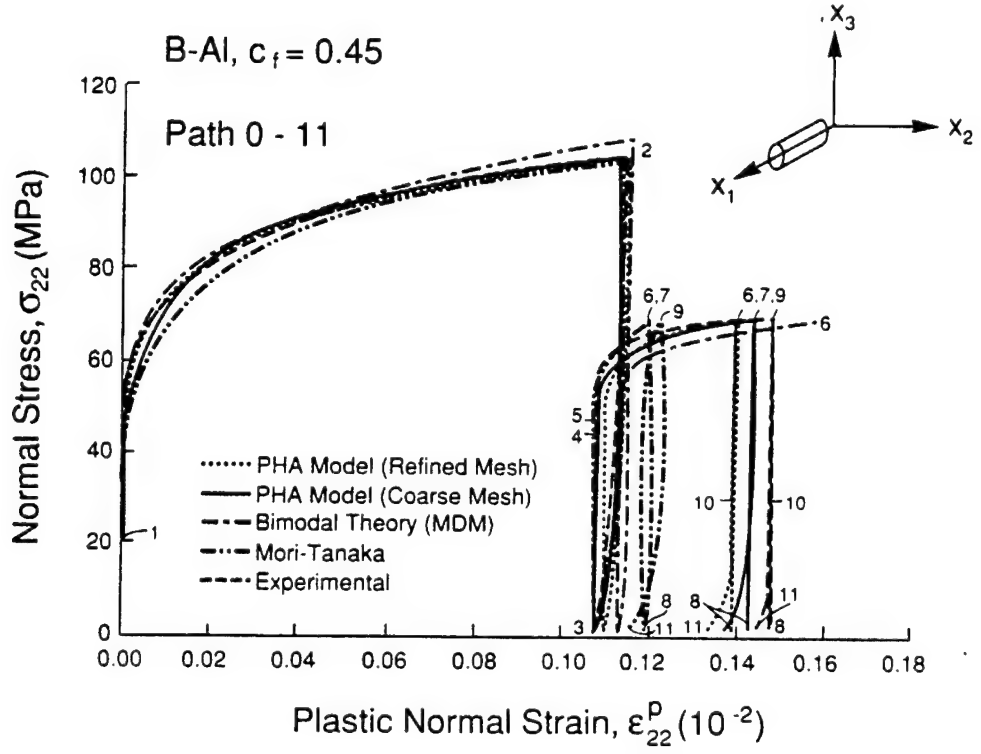

Figure 7 Comparison of measured and predicted transverse normal stress-plastic strain response of the composite tube during loading along the path 0–11 of Figure 6.

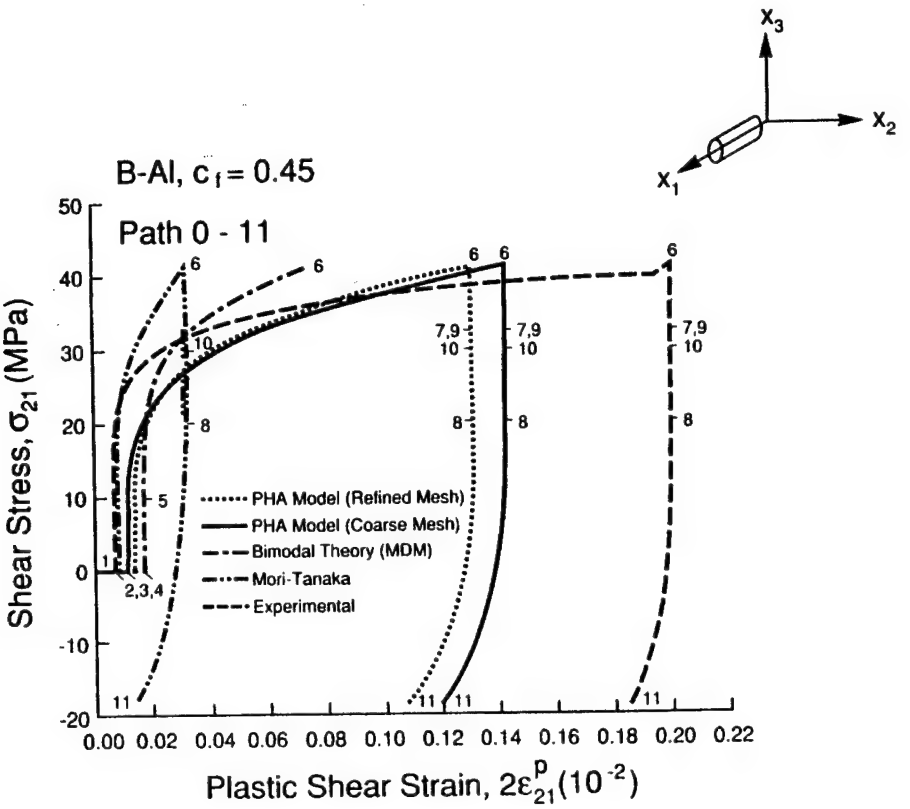

Figure 8 Comparison of measured and predicted longitudinal shear stress-plastic strain response of the composite tube during loading along the path 0–11 of Figure 6.

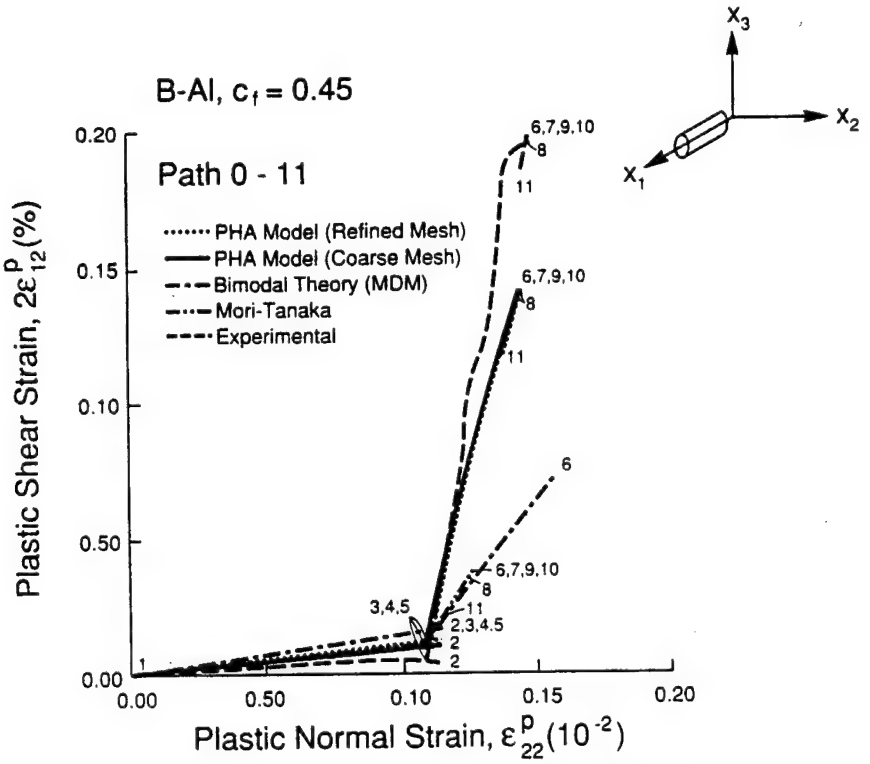

Figure 9 Comparison of measured and predicted plastic normal strain-shear strain path caused by loading along the path 0–11 of Figure 6.

has a significant effect on the nonlinear response of the phases. We begin with a brief summary of the rate-dependent constitutive equations for homogeneous phases, and follow with the solution for composite materials subjected to thermomechanical loads.

1.14.4.1 Viscoplasticity of Homogeneous Materials

Several theories have been postulated to model the viscoplastic behavior of homogeneous materials (Bodner and Partom, 1975; Liu and Krempl, 1979; Eisenberg and Yen, 1981; Walker, 1981; Chaboche, 1989; Neu, 1993). In a high temperature environment, certain features of the response, such as thermal hardening and recovery, must be included. To represent *in situ* behavior of the homogeneous phases of composite materials, the constitutive equations must adequately model the response under nonproportional loads. Several of these features are captured by the theories found in the literature. Here, we briefly describe a rate-dependent theory with a yield surface which was developed by the authors (Bahei-El-Din *et al.*, 1991), and implemented in micromechanical models of composite materials (Bahei-El-Din *et al.*, 1991; Bahei-El-Din, 1994, 1996) subjected to thermomechanical loads. For isothermal, proportional loading regimes, the theory degenerates to the equations proposed by Eisenberg and Yen (1981).

Assuming that the elastic response is rate-insensitive, a yield surface which bounds all stress states that produce pure elastic strains is postulated in the general form in Equation (30), or the Mises form in Equation (31). The latter is rewritten here in terms of the deviatoric equilibrium stress, which represents the long-term stress state that will be attained by the material under constant strain induced by loading at a certain time rate. Accordingly, the corresponding yield surface is referred to as the equilibrium surface. If both kinematic and isotropic hardening are considered, the Mises equilibrium surface is written as

$$f \equiv \frac{3}{2}(\boldsymbol{s}^* - \boldsymbol{a}) : (\boldsymbol{s}^* - \boldsymbol{a}) - (Y(T) + \Omega)^2 = 0 \qquad (83)$$

where $\boldsymbol{s}^*$ is the deviatoric equilibrium stress tensor, $\boldsymbol{a}$ denotes the center of the equilibrium yield surface, $Y \equiv Y(T)$ is the initial yield stress in tension, and $\Omega \equiv \Omega(T)$ is an isotropic hardening function.

For a given deviatoric stress tensor $\boldsymbol{s}$, which lies outside the yield surface in Equation (83), there exists an equilibrium stress $\boldsymbol{s}^*$ which satisfies Equation (83) and is collinear with $\boldsymbol{s}$ and $\boldsymbol{a}$. Hence,

$$\boldsymbol{s}^* = \left(\frac{2(Y+\Omega)^2}{3(\boldsymbol{s}^* - \boldsymbol{a}) : (\boldsymbol{s}^* - \boldsymbol{a})}\right)^{\frac{1}{2}} (\boldsymbol{s}^* - \boldsymbol{a}) + \boldsymbol{a} \qquad (84)$$

The effective overstress Λ is a measure of the distance between the actual stress point $\boldsymbol{s}$ and the equilibrium point $\boldsymbol{s}^*$. It vanishes if the stress point lies on, or falls inside the yield surface. In particular,

$$\Lambda = \left(\frac{3}{2}(\boldsymbol{s} - \boldsymbol{s}^*) : (\boldsymbol{s} - \boldsymbol{s}^*)\right)^{\frac{1}{2}} \text{ if } f(\boldsymbol{s} - \boldsymbol{a}) > 0 \qquad (85)$$

$$\Lambda = 0 \qquad \text{if } f(\boldsymbol{s} - \boldsymbol{a}) \leqslant 0 \qquad (86)$$

If the overstress is nonzero, Equation (85), inelastic strains develop at the rate

$$\dot{\boldsymbol{\varepsilon}}^{\text{in}} = \left(\sqrt{\frac{3}{2}} k(T) \Lambda^{p(T)}\right) \mathbf{n} \qquad (87)$$

where the functions $k(T)$ and $p(T)$ are material parameters and $\mathbf{n}$ is a unit normal to the yield surface in Equation (83) at the current equilibrium stress point. The latter is found from Equation (83) as (see also Equation (43))

$$\mathbf{n} = \frac{1}{\sqrt{\frac{2}{3}}(Y+\Omega)} \begin{bmatrix} \hat{s}_{11} & \hat{s}_{22} & \hat{s}_{33} & 2\hat{s}_{23} & 2\hat{s}_{31} & 2\hat{s}_{12} \end{bmatrix}^{\mathrm{T}} \qquad \hat{\boldsymbol{s}} = \boldsymbol{s}^* - \boldsymbol{a} \qquad (88)$$

The time rate of Ω is dependent on inelastic deformation and thermal recovery of the equilibrium yield surface. It is given by

$$\dot{\Omega} = \omega(T) [\Omega_a(T) - \Omega] \dot{\bar{\varepsilon}}^{\text{in}} - b_r(T) |\Omega - \Omega_r(T)|^{(\rho_r(T)-1)} [\Omega - \Omega_r(T)] \qquad (89)$$

The functions $\omega(T)$, $\Omega_a(T)$, $b_r(T)$, $\Omega_r(T)$ and $\rho_r(T)$ are material parameters, and $\dot{\bar{\varepsilon}}^{\text{in}}$ is the effective inelastic strain rate;

$$\dot{\bar{\varepsilon}}^{\text{in}} = \left[\frac{2}{3}\dot{\boldsymbol{\varepsilon}}^{\text{in}} : \dot{\boldsymbol{\varepsilon}}^{\text{in}}\right]^{\frac{1}{2}} = k(T)\Lambda^{p(T)}, \quad \dot{\varepsilon}^{\text{in}}_{kk} = 0 \qquad (90)$$

Total ($\Omega_r = 0$), or partial ($\Omega_r \neq 0$) thermal recovery is represented by the second term in Equation (89).

In analogy with Equation (89), and permitting complete thermal recovery of kinematic hardening, the evolution equation for the center of the equilibrium yield surface can be written as

$$\dot{\boldsymbol{\sigma}} = \dot{\gamma}\boldsymbol{\nu} - \eta_r(T)\bar{\sigma}^{(\chi_r(T)-1)}\boldsymbol{\sigma}, \quad \bar{\sigma} = (\boldsymbol{\sigma}:\boldsymbol{\sigma})^{1/2} \tag{91}$$

where $\eta_r(T)$ and $\chi_r(T)$ are material parameters. The unit tensor $\boldsymbol{\nu}$ defines the direction of translation of the yield surface in the deviatoric stress space, and can be specified according to the hardening rules applied in rate-independent plasticity theories. If the Phillips hardening rule is selected, then

$$\boldsymbol{\nu} = \frac{\dot{\boldsymbol{\sigma}}}{(\dot{\boldsymbol{\sigma}}:\dot{\boldsymbol{\sigma}})^{1/2}} \quad \text{if} \quad \dot{\boldsymbol{\sigma}} \neq 0 \tag{92}$$

$$\boldsymbol{\nu} = \mathbf{n} \text{ if } \dot{\boldsymbol{\sigma}} = 0 \tag{93}$$

The factor $\dot{\gamma}$ in Equation (91) is found from Prager's consistency condition $\dot{f} = 0$, when translation of the yield surface is specified by the first term in Equation (91). The result is

$$\dot{\gamma} = \sqrt{2/3}k(T)\Lambda^{p(\mathrm{T})}[H(T) - \omega(T)(\Omega_a(T) - \Omega)]\Big/(\mathbf{n}:\boldsymbol{\nu}) \tag{94}$$

A two-surface plasticity theory (Dafalias and Popov, 1976) can be used to describe evolution of the instantaneous tangent modulus H. In analogy with Equation (83), a bounding surface is postulated in the form

$$g \equiv \frac{3}{2}(\bar{\boldsymbol{\sigma}} - \bar{\boldsymbol{\alpha}}):(\bar{\boldsymbol{\sigma}} - \bar{\boldsymbol{\alpha}}) - \left(\bar{Y}(T) + \bar{\Omega}\right)^2 = 0 \tag{95}$$

where $\bar{\boldsymbol{\sigma}}$ is the deviatoric bounding stress tensor, determined from equality of the normal to the equilibrium yield surface $\mathbf{n}(\boldsymbol{\sigma}^* - \boldsymbol{\alpha})$, Equation (88), and the normal to the bounding surface $\mathbf{n}(\bar{\boldsymbol{\sigma}} - \bar{\boldsymbol{\alpha}})$, and $\bar{\boldsymbol{\alpha}}$ is the center of the bounding surface. $\bar{Y}(T)$ denotes the bounding stress, given by the intersection of the asymptotic part of the uniaxial stress–strain curve and the stress axis, and $\bar{\Omega} = \bar{\Omega}(T)$ is an isotropic hardening function. The instantaneous tangent modulus is then given by

$$H(T) = H_o(T) + h(T)\left(\frac{\delta}{\delta_o - \delta}\right)^{\xi(T)}$$
$$\delta = \left(\frac{3}{2}(\bar{\boldsymbol{\sigma}} - \boldsymbol{\sigma}^*):(\bar{\boldsymbol{\sigma}} - \boldsymbol{\sigma}^*)\right)^{1/2} \tag{96}$$

where δ_o is the distance between the equilibrium yield surface and the bounding surface at the onset of inelastic deformation. When the equilibrium stress point lies on the bounding surface, $\delta = 0$, and the plastic tangent modulus $H(T)$ assumes the asymptotic value $H_o(T)$, which together with the parameters $h(T)$ and $\xi(T)$ need to be determined experimentally.

In analogy with the equilibrium yield surface, thermal recovery of isotropic, as well as kinematic, hardening of the bounding surface can be included in the model. This is omitted here for brevity. We only mention that the recovery terms for isotropic and kinematic hardening of the bounding surface assume a form similar to those suggested above for the equilibrium surface, but with new material parameters.

With the above constitutive law, we can now write the stress–strain rate equations in the form suggested in Equation (4);

$$\dot{\boldsymbol{\sigma}} = \mathbf{L}\dot{\boldsymbol{\varepsilon}} + \dot{\boldsymbol{\lambda}}, \quad \dot{\boldsymbol{\varepsilon}} = \mathbf{M}\dot{\boldsymbol{\sigma}} + \dot{\boldsymbol{\mu}} \tag{97}$$

where

$$\mathbf{L} = \mathbf{M}^{-1}, \quad \dot{\boldsymbol{\lambda}} = -\mathbf{L}\dot{\boldsymbol{\mu}} \tag{98}$$

$$\dot{\boldsymbol{\mu}} = \dot{\boldsymbol{\varepsilon}}^{\mathrm{in}} + \boldsymbol{\alpha}\dot{T} = \left(\sqrt{\frac{3}{2}}k(T)\Lambda^{p(\mathrm{T})}\right)\mathbf{n} + \boldsymbol{\alpha}\dot{T} \tag{99}$$

and $\mathbf{n}$ is given by Equation (88).

1.14.4.2 Viscoplasticity of Composite Materials

Equations (97)–(99) can be applied to each viscoplastic phase or subvolume of a composite representative volume V to compute the local fields and the overall response. This is achieved by the transformation field analysis, which employs Equation (10) to compute increments of the local stresses as the sum of contributions from the overall load and the local transformation strains. Substituting Equation (99) into Equation (10), we obtain the stress rate in volume V_r as

$$\dot{\boldsymbol{\sigma}}_r = \mathbf{B}_r\dot{\boldsymbol{\sigma}} - \sum_{s=1}^{Q}\left(\sqrt{\frac{3}{2}}k_s(T)\Lambda_s^{p_s(\mathrm{T})}\right)\mathbf{F}_{rs}\mathbf{L}_s\mathbf{n}_s - \sum_{s=1}^{Q}\mathbf{F}_{rs}\mathbf{L}_s\boldsymbol{\alpha}_s\dot{T}, r = 1, 2, \ldots Q \tag{100}$$

Integration of Equation (100) along the loading path $(\dot{\boldsymbol{\sigma}}, \dot{\theta})$ provides the local stresses. The local strain increments are found from Equations (97) and (99), and the overall inelastic strain increments from the generalized Levin's formula in Equation (11).

This approach is applicable to both the averaging models ($Q = 2$) in Section 1.14.2.2.1, and the periodic array models ($Q > 2$) in Section 1.14.2.2.2. Selection of a particular model is reflected in the form of the stress concentration factors $\mathbf{B}_r$ and influence functions $\mathbf{F}_{rs}$. Dvorak *et al.* (1994) illustrate the application of this

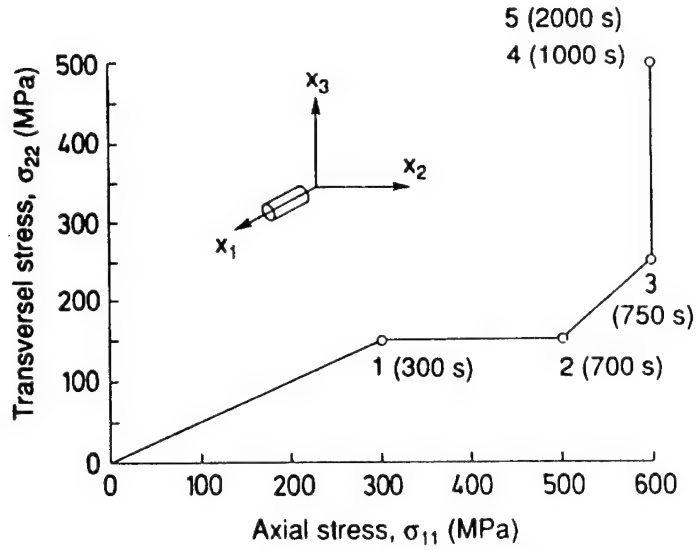

Figure 10 Axial tension–transverse tension path applied to a SCS6/Ti-15-3 composite.

method to unidirectional composites with a viscoplastic matrix.

Solution of thermo-viscoplastic problems of periodic array models can be also obtained by the finite element method. This is described by Bahei-El-Din (1996) and implemented in the Viscopac code (Bahei-El-Din, 1994).

1.14.4.3 Application

To illustrate the procedure described above, we examine the time-dependent response of a high-temperature metal matrix composite. The composite material consists of a titanium matrix (Ti-15-3) reinforced with a silicon carbide fiber (SCS6) at 30 volume percent, and was examined at 482° C. At this temperature, the fiber is assumed to be elastic, and the matrix elastic-viscoplastic with constitutive behavior described by the constitutive law given in Section 1.14.4.1. Johnson *et al.* (1993) give material properties of the constituents.

The unit cell derived from the periodic hexagonal array model (Figures 1(b) and 2), was subdivided into 16 elements, 10 in the matrix and 6 in the fiber. The finite element method was then used to compute the mechanical and transformation concentration factors $\mathbf{B}_r$ and $\mathbf{F}_{rs}$. Equation (100) and the evolution equations for the viscoplastic matrix in Section 1.14.4.1, were integrated for a specified overall stress path (Dvorak *et al.*, 1994).

The loading consisted of axial and transverse normal stresses, σ_{11} and σ_{22}, which were combined as shown in Figure 10 and applied at the rates given in Figure 11. The corresponding overall strains, ε_{11} and ε_{22}, are plotted in Figure 12. The effect of the time-dependent deformation of the matrix is evident, particularly at the sustained stress in the time segment 4–5. It is seen that overall creep strains are developed in both the axial and transverse directions, albeit at different rates.

1.14.5 INELASTIC LAMINATES

In this section, we describe analysis of fibrous composite laminates with inelastic phases using micromechanical models for the unidirectional plies. The approach expands the transformation field analysis to laminates and evaluates the instantaneous response of the laminate as well as the stresses and strains in the individual plies and their phases. This is achieved by regarding the laminate as an aggregate of homogeneous phases with constraints derived from a micromechanical model of the ply, and the in-plane equi-strain condition found in laminates.

First, we find the lamina overall stresses as a function of the applied load and the lamina transformation strains. Next, we proceed to evaluate the local stresses in the phases of the individual plies using two approaches. In one approach, the transformation field analysis is used to formulate rate equations for the phase stresses in all plies in terms of phase and ply concentration factors and influence functions. Either averaging models or periodic array models can be utilized. In the other approach, developed for laminates in which the individual plies possess a periodic microstructure, the lamina stresses are applied to a unit cell of the ply, and the local stresses are computed with the finite element method.

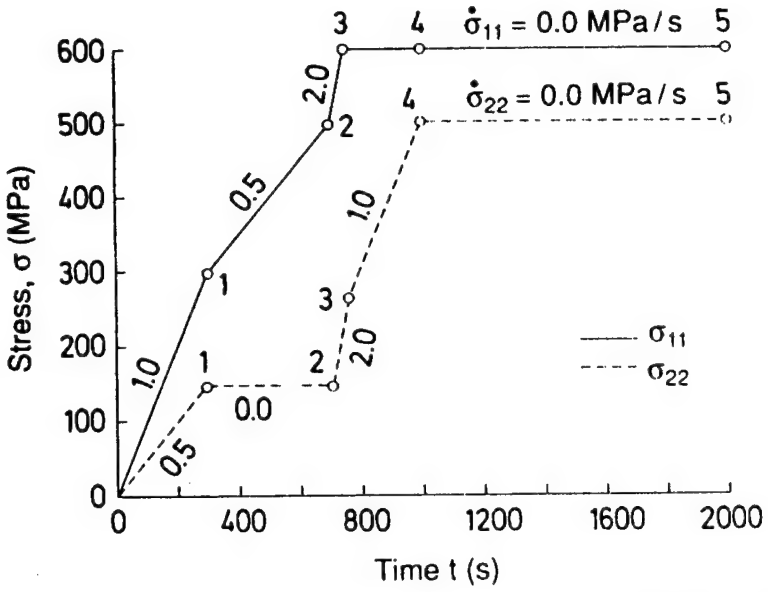

Figure 11 Time history corresponding to the loading path of Figure 10.

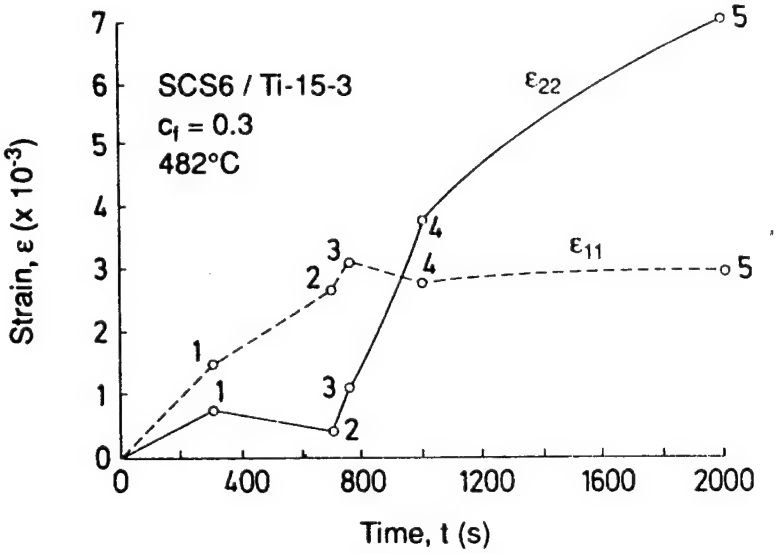

Figure 12 Overall strain histories computed for the loading path of Figures 10 and 11.

1.14.5.1 Lamina Stresses

The behavior of a symmetric laminated plate consisting of $2N$ fully bonded thin elastic plies under thermomechanical loads is considered (Figure 13). Referred to a Cartesian coordinate system, x_k, $k = 1, 2, 3$, in which the x_1 x_2-plane coincides with the midplane of the laminate, in-plane membrane forces and the corresponding uniform stresses, σ_{11}, σ_{22}, and σ_{12} are applied, together with a uniform normal stress, σ_{33}, in the thickness direction x_3. The out-of-plane normal stress can be found in applications that involve pressure loading, such as in fabrication by isostatic pressing. $\boldsymbol{\sigma} = [\sigma_{11}, \sigma_{22}, \sigma_{12}]$ lists the in-plane stresses applied to the laminate, and $\boldsymbol{\varepsilon} = [\varepsilon_{11}, \varepsilon_{22}, 2\varepsilon_{12}]$ lists the corresponding laminate strains. The latter are caused by the applied stresses, $\boldsymbol{\sigma}$ and σ_{33} in addition to the transformation strains generated in the individual plies, such as thermal and inelastic strains, which are not recovered by removal of the mechanical load.

Assuming additive decomposition of the various effects (Dvorak, 1991), and adopting the notation of Bahei-El-Din (1992), the time rates

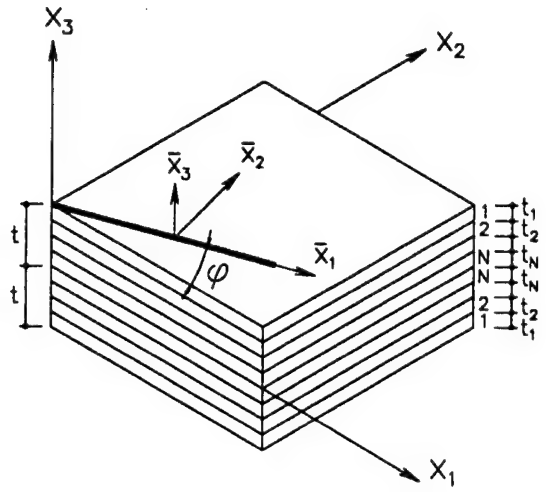

Figure 13 Geometry of a symmetric fibrous laminate.

of the laminate in-plane stresses and strains are written as

$$\dot{\boldsymbol{\sigma}} = \mathbf{L}\dot{\boldsymbol{\varepsilon}} + \mathbf{k}\dot{\sigma}_{33} + \dot{\boldsymbol{\lambda}} \tag{101}$$

$$\dot{\boldsymbol{\varepsilon}} = \mathbf{M}\dot{\boldsymbol{\sigma}} + \mathbf{f}\dot{\sigma}_{33} + \dot{\boldsymbol{\mu}} \tag{102}$$

where $\boldsymbol{\lambda} = [\lambda_{11}, \lambda_{22}, \lambda_{12}]$ and $\boldsymbol{\mu} = [\mu_{11}, \mu_{22}, 2\mu_{12}]$ are the in-plane transformation stress and strain, respectively, and $\mathbf{L}$ and $\mathbf{M}$ are the elastic stiffness and compliance matrices for in-plane loading. The $\mathbf{k}$ vector lists the in-plane stresses caused in the laminate by a unit out-of-plane normal stress, $\sigma_{33} = 1$, in the absence of both the total in-plane strain $\boldsymbol{\varepsilon}$, and transformation stress $\boldsymbol{\lambda}$, whereas $\mathbf{f}$ is the elastic compliance vector associated with the out-of-plane normal stress, σ_{33}. On the other hand, the transformation strain $\boldsymbol{\mu}$ represents the total strain that remains in the laminate after complete unloading to zero stress, and the transformation stress $\boldsymbol{\lambda}$ is seen to represent the total stress caused in a fully constrained laminate by the transformation strain $\boldsymbol{\mu}$. Equations (101) and (102) provide the relations,

$$\mathbf{L} = \mathbf{M}^{-1}, \quad \mathbf{k} = -\mathbf{L}\mathbf{f}, \quad \boldsymbol{\lambda} = -\mathbf{L}\boldsymbol{\mu} \tag{103}$$

In analogy with Equations (101) and (102), the uniform in-plane stress and strain rates of a ply (i), $i = 1, 2, \ldots, N$, in the local coordinate system $\bar{x}_k$, $k = 1,2,3$ (Figure 13), can be written as,

$$\dot{\bar{\boldsymbol{\sigma}}}_i = \mathbf{L}_i\dot{\bar{\boldsymbol{\varepsilon}}}_i + \mathbf{k}_i\dot{\bar{\sigma}}^i_{33} + \dot{\bar{\boldsymbol{\lambda}}}_i \tag{104}$$

$$\dot{\bar{\boldsymbol{\varepsilon}}}_i = \mathbf{M}_i\dot{\bar{\boldsymbol{\sigma}}}_i + \mathbf{f}_i\dot{\bar{\sigma}}^i_{33} + \dot{\bar{\boldsymbol{\mu}}}_i \tag{105}$$

where $\bar{\mathbf{L}}_i$ and $\bar{\mathbf{M}}_i$ are the elastic stiffness and compliance matrices for in-plane loading, $\bar{\mathbf{k}}_i$ and $\bar{\mathbf{f}}_i = -\bar{\mathbf{M}}_i\,\bar{\mathbf{k}}_i$ are the ply in-plane stress and strain caused by a unit out-of-plane normal stress, and $\bar{\boldsymbol{\lambda}}_i$ and $\bar{\boldsymbol{\mu}}_i = -\bar{\mathbf{M}}_i\,\bar{\boldsymbol{\lambda}}_i$ are the ply in-plane transformation stress and strain. For a transversely isotropic ply with overall elastic longitudinal, and transverse moduli, E_L and E_T, Poisson's ratios, ν_L and ν_T, and longitudinal shear modulus G_L, the matrices found in Equations (104) and (105) are given by (Bahei-El-Din, 1992; Dvorak and Bahei-El-Din, 1995),

$$\mathbf{L}_i = \frac{1}{k+m}\begin{bmatrix} E_L k + mn & 2m\ell & 0 \\ 2m\ell & 4km & 0 \\ 0 & 0 & p(k+m) \end{bmatrix} = \mathbf{M}_i^{-1}$$

$$\mathbf{k}_i = \frac{1}{k+m}\begin{bmatrix} \ell \\ k-m \\ 0 \end{bmatrix} \tag{106}$$

$$\mathbf{M}_i = \begin{bmatrix} 1/E_L & -\nu_L/E_L & 0 \\ -\nu_L/E_L & 1/E_T & 0 \\ 0 & 0 & 1/G_L \end{bmatrix}$$

$$\mathbf{f}_i = \begin{bmatrix} -\nu_L/E_L \\ -\nu_T/E_T \\ 0 \end{bmatrix} = -\mathbf{M}_i\mathbf{k}_i \tag{107}$$

where k, ℓ, m, n, and p are Hill's (1964) moduli (see Section 1.14.8), and $E_L = n - \ell^2/k$, $\nu_L = l/2k$, $m = E_T/2(1 + \nu_T)$, $G_L = p$.

When expressed in the overall coordinate system x_k, $k = 1, 2, 3$, Equations (104) and (105) are written as (Bahei-El-Din, 1992)

$$\dot{\boldsymbol{\sigma}}_i = \mathbf{L}_i\dot{\boldsymbol{\varepsilon}}_i + \mathbf{k}_i\dot{\sigma}^i_{33} + \dot{\boldsymbol{\lambda}}_i \tag{108}$$

$$\dot{\boldsymbol{\varepsilon}}_i = \mathbf{M}_i\dot{\boldsymbol{\sigma}}_i + \mathbf{f}_i\dot{\sigma}^i_{33} + \dot{\boldsymbol{\mu}}_i \tag{109}$$

where

$$\dot{\bar{\boldsymbol{\sigma}}}_i = \mathbf{R}_i\dot{\boldsymbol{\sigma}}_i, \dot{\bar{\sigma}}^i_{33} = \dot{\sigma}^i_{33}, \dot{\bar{\boldsymbol{\varepsilon}}}_i = \mathbf{N}_i\dot{\boldsymbol{\varepsilon}}_i \tag{110}$$

$$\dot{\boldsymbol{\lambda}}_i = \mathbf{R}_i\dot{\boldsymbol{\lambda}}_i = -\mathbf{L}_i\dot{\boldsymbol{\mu}}_i, \dot{\boldsymbol{\mu}}_i = \mathbf{N}_i\dot{\boldsymbol{\mu}}_i \tag{111}$$

$$\mathbf{L}_i = \mathbf{N}_i^T\mathbf{L}_i\mathbf{N}_i = \mathbf{M}_i^{-1}, \mathbf{k}_i = \mathbf{N}_i^T\mathbf{k}_i = -\mathbf{L}_i\mathbf{f}_i \tag{112}$$

$$\mathbf{R}_i^T = \mathbf{N}_i^{-1} = \begin{bmatrix} \cos^2\varphi_i & \sin^2\varphi_i & -\frac{1}{2}\sin 2\varphi_i \\ \sin^2\varphi_i & \cos^2\varphi_i & \frac{1}{2}\sin 2\varphi_i \\ \sin 2\varphi_i & -\sin 2\varphi_i & \cos 2\varphi_i \end{bmatrix} \tag{113}$$

and ϕ_i is the angle between the local $\overline{x}_1$-axis and the overall x_1-axis (Figure 13).

The ply stresses in a laminate loaded by overall in-plane stress $\boldsymbol{\sigma}$, out-of-plane normal stress σ_{33}, and ply transformation stress $\boldsymbol{\lambda}_i$, introduced by certain prescribed in-plane transformation strains $\boldsymbol{\mu}_i = -\mathbf{M}_i\boldsymbol{\lambda}_i$, can now be determined using the transformation field analysis method. The laminate is regarded as elastic, and the ply in-plane stress is written as the sum of the overall stress and local transformation stress contributions (Dvorak and Bahei-El-Din, 1995). On the other hand, the normal stress in the thickness direction equals the applied stress. Hence,

$$\dot{\boldsymbol{\sigma}}_i = \mathbf{H}_i\dot{\boldsymbol{\sigma}} + \boldsymbol{\kappa}_i\dot{\sigma}_{33} + \sum_{j=1}^{N}\mathbf{K}_{ij}\dot{\boldsymbol{\lambda}}_j, \dot{\sigma}_{33}^i = \dot{\sigma}_{33} \qquad i = 1,2,..N \tag{114}$$

We note that the lamina out-of-plane transformation stresses λ_{33}, λ_{13}, and λ_{23} do not necessarily vanish, but they are not introduced in Equation (114) since the in-plane equi-strain condition imposed on the perfectly bonded plies can be maintained under these transformation stresses without introducing additional ply stresses. The $\mathbf{H}_i$ and $\boldsymbol{\kappa}_i$ matrices are stress distribution factors for in-plane overall stresses, and out-of-plane normal stress, respectively, and $\mathbf{K}_{ij}$ is a transformation influence function. The kth column of matrix $\mathbf{K}_{ij}$ provides the in-plane stresses, σ_{11}, σ_{22}, and σ_{12} caused in lamina (i) by a unit transformation stress λ_k, k = 1,2,3, applied to lamina (j) while the overall stresses $\boldsymbol{\sigma}$ and σ_{33} are absent.

The distribution factors $\mathbf{H}_i$ and $\boldsymbol{\kappa}_i$, and the influence coefficients $\mathbf{K}_{ij}$ are evaluated by realizing the in-plane strain compatibility of the perfectly bonded plies, $\boldsymbol{\varepsilon} = \boldsymbol{\varepsilon}_i$, and the force equilibrium condition, $\sum c_i\,\boldsymbol{\sigma}_i = \boldsymbol{\sigma}$, i = 1,2,.. N, where $c_i = t_i/t$ (see Figure 13) is the volume fraction of the ply. From these conditions, and using Equation (114), one can establish that

$$\mathbf{H}_i = \mathbf{L}_i\mathbf{M}, \quad \boldsymbol{\kappa}_i = \mathbf{L}_i(\mathbf{f} - \mathbf{f}_i) \tag{115}$$

$$\mathbf{M} = \mathbf{L}^{-1}, \quad \mathbf{L} = \sum_{i=1}^{N} c_i\mathbf{L}_i \tag{116}$$

$$\mathbf{f} = -\mathbf{M}\mathbf{k}, \quad \mathbf{k} = \sum_{i=1}^{N} c_i\mathbf{k}_i \tag{117}$$

$$\mathbf{K}_{ij} = \delta_{ij}\,\mathbf{I} - \mathrm{c}_j\,\mathbf{H}_i \tag{118}$$

where δ_{ij} is Kronecker's tensor, $\mathbf{I}$ is the identity matrix, and

$$\sum_{i=1}^{N} c_i\mathbf{H}_i = \mathbf{I}, \sum_{i=1}^{N} c_i\boldsymbol{\kappa}_i = \mathbf{0} \tag{119}$$

1.14.5.2 Transformation Field Analysis Method

We now consider evaluation of the phase stress rates in each lamina using the governing equations presented in the preceding section, when the plies are subjected to the stress in Equation (114). Since we are primarily concerned with transformation strains of thermal and inelastic type, we first substitute the lamina transformation stress $\boldsymbol{\lambda}_j$ in Equation (114) in terms of the eigenstrains as $\boldsymbol{\lambda}_j = -\mathbf{L}_j\boldsymbol{\mu}_j$, and use Equation (111) to transform the strain $\boldsymbol{\mu}_j$ into the lamina local coordinates. Next, the ply overall stress in Equation (114) is transformed into the local coordinate system of the ply using Equation (110). Hence, the ply stresses in local coordinates is written as

$$\dot{\bar{\boldsymbol{\sigma}}}_i = \mathbf{R}_i\mathbf{H}_i\dot{\boldsymbol{\sigma}} + \mathbf{R}_i\mathbf{k}_i\dot{\sigma}_{33} - \mathbf{R}_i\sum_{j=1}^{N}\mathbf{K}_{ij}\mathbf{L}_{ij}\mathbf{R}_j^T\dot{\bar{\boldsymbol{\mu}}}_j$$
$$\dot{\bar{\sigma}}_{33}^i = \dot{\sigma}_{33}, \quad i = 1,2,..N \tag{120}$$

Given the lamina stress referred to the material axes, Equation (120), the local stresses in the phases of the individual plies are determined using the procedure described in Section 1.14.2. A representative volume V_j of a unidirectional composite ply (j), j = 1,2,..., N, is selected and divided into subvolumes V_η^j, η = 1,2,..., Q, such that $V_j = \sum V_\eta^j$. The number of subvolumes Q depends on the micromechanical model selected for the lamina. For two-phase averaging models, Section 1.14.2.2.1, the number of subvolumes is two representing the matrix and the fiber. On the other hand, representative volumes derived from periodic array models, Section 1.14.2.2.2, may contain several subvolumes in each of the fiber and matrix phases. From Equation (10), the local stresses in the subvolumes of lamina (i) are written as a (6 × 1) vector in the form

$$\dot{\boldsymbol{\sigma}}_\rho^i = \hat{\mathbf{B}}_\rho^i \dot{\bar{\boldsymbol{\sigma}}}_i + \mathbf{b}_\rho^i \dot{\bar{\sigma}}_{33}^i - \sum_{\eta=1}^{Q} \mathbf{F}_{\rho\eta}^i \mathbf{L}_\eta^i \dot{\boldsymbol{\mu}}_\eta^i \qquad (121)$$
$$\rho = 1,2,..Q, \quad i = 1,2,..N$$

The first two terms represent, respectively, the local stress used by the ply in-plane stresses and out-of-plane normal stress. The (6×3) $\hat{\mathbf{B}}_\rho^i$ matrix, and the (6×1) $\mathbf{b}_\rho^i$ vector are stress concentration factor given by the respective partitions of the regular (6×6) stress concentration factor $\mathbf{B}_\rho^i$ after the columns of the latter are reordered according to the stress labels 11, 22, 12, 33, 13, 23. The last term in Equation (121) is the local stress caused by the phase transformation strains.

The lamina transformation strain is given in terms of their local counterparts by the Levin's formula in Equation (11), written here for the in-plane components;

$$\dot{\boldsymbol{\mu}}_j = \sum_{\eta=1}^{Q} \bar{c}_\eta^j \left[\hat{\mathbf{B}}_\eta^j\right]^T \dot{\boldsymbol{\mu}}_\eta^j, \bar{c}_\eta^j = V_\eta^j / V_j, \quad j = 1,2,..N \qquad (122)$$

From Equations (120)–(122), the local stresses in the plies can be written as

$$\dot{\boldsymbol{\sigma}}_\rho^i = \hat{\mathbf{B}}_\rho^i \mathbf{R}_i \mathbf{H}_i \dot{\boldsymbol{\sigma}} + \left(\hat{\mathbf{B}}_\rho^i \mathbf{R}_i \boldsymbol{\kappa}_i + \mathbf{b}_\rho^i\right) \dot{\sigma}_{33} - \sum_{\eta=1}^{Q} \mathbf{F}_{\rho\eta}^i \mathbf{L}_\eta^i \dot{\boldsymbol{\mu}}_\eta^i$$
$$- \hat{\mathbf{B}}_\rho^i \mathbf{R}_i \sum_{j=1}^{N} \mathbf{K}_{ij} \mathbf{L}_{ij} \mathbf{R}_j^T \left[\sum_{\eta=1}^{Q} \bar{c}_\eta^j \left[\hat{\mathbf{B}}_\eta^j\right]^T \dot{\boldsymbol{\mu}}_\eta^j\right]$$
$$\rho = 1,2,..Q, i = 1,2,..N \qquad (123)$$

The first and second terms in Equation (123) provide, respectively, the local stress caused by the overall in-plane stresses and out-of-plane normal stress applied to the laminate, while the last two terms are the contributions of the subvolume transformation strains in all plies to the subvolume ρ of lamina (i). The third term provides the local stresses due to local transformation strains in lamina (i). The in-plane constraint $\boldsymbol{\varepsilon} = \boldsymbol{\varepsilon}_i$ imposed on the lamina causes additional stresses in the subvolumes of the plies when transformation strains $\dot{\boldsymbol{\mu}}_\eta^j$ are present in other layers (j). This effect is given by the last term in Equation (123).

Considering a specific form for the phase transformation strains, derived for example from thermal and viscoplastic strains in Equation (99), the rate equations provided by Equation (123) for the local stresses in all plies can be integrated along a specified loading path ($\boldsymbol{\sigma}$, σ_{33}, T) applied to the laminate. If the phase elastic moduli change with temperature, the local stress concentration factors and influence coefficients in all plies must be updated within the integration process. Wafa (1994) gives examples of laminate analysis using this approach.

1.14.5.3 Finite Element/Transformation Analysis Method

In this method, inelastic analysis of laminates is performed considering a detailed representation of the microstructure of each ply using a unit cell model. While the analysis on the microscale is performed with the finite element method, the stress rates for each ply are obtained from a transformation field analysis of the laminated plate (Bahei-El-Din *et al.*, 1998). In this way, local phenomena related to the plies are incorporated in the finite element solution, while the corresponding overall ply deformation is accounted for in the laminate analysis.

Transformation field analysis of the laminates follows the procedure described in the preceding section, leading to Equation (120). This provides the stress rates, $\dot{\bar{\sigma}}_{11}^i$, $\dot{\bar{\sigma}}_{22}^i$, $\dot{\bar{\sigma}}_{33}^i$, and $\dot{\bar{\sigma}}_{12}^i$, $i = 1,2,\ldots, N$, for the plies, referred to their local coordinate system. Response of the unit cell representing each lamina under these stresses is computed with the finite element method. For example, if the unit cell derived from the PHA model is selected (Figure 2), the rates of nodal forces equivalent to the lamina stress rates are computed from Equation (27) and applied at the degrees of freedom indicated in Figure 2.

Considering viscoplastic phases, augmentation of the finite element procedure with Equation (120) provides a system of first order differential equations (ODE) in the form (Bahei-El-Din *et al.*, 1998),

$$\dot{y}_j(t) = g_j(t, y_1, y_2, ..., y_R) \qquad (124)$$

The unknown functions g_j, $j = 1, 2,\ldots, R$, are identified with the laminate overall strain $\boldsymbol{\varepsilon}$, ply stresses $\boldsymbol{\sigma}_i$ and σ_{33}^i in the overall axes, and transformation strain $\boldsymbol{\mu}_i$, $i = 1, 2,\ldots, N$, phase stress $\boldsymbol{\sigma}_\eta$ and transformation strain $\boldsymbol{\mu}_\eta$, $\eta = 1, 2,\ldots, Q$ in all N plies. The unknown functions also include the nodal displacements for the unit cell of each ply and any internal variables required to define the rate-dependent deformation of the phases, e.g. the overstress in Equation (85). Assuming elastic response of the phases in the initial state, Equation (124) can be integrated over a specified time period using an ODE solver that is appropriate for stiff differential equations which are usually encountered in viscoplastic response modeled with the power law assumed in Equation (87).

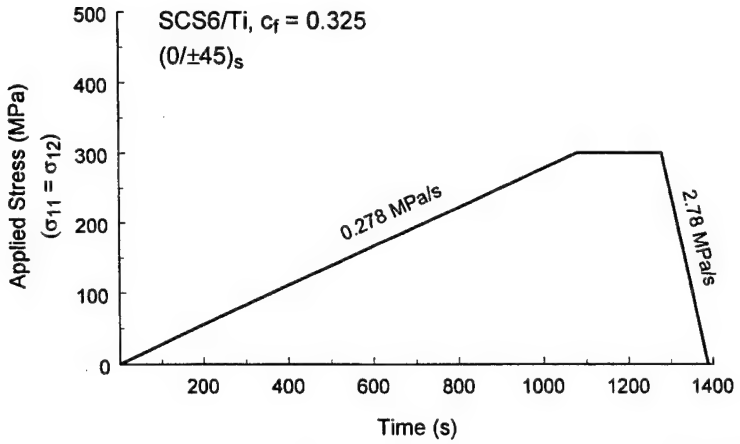

Figure 14 Loading history applied to a high-temperature metal matrix laminate.

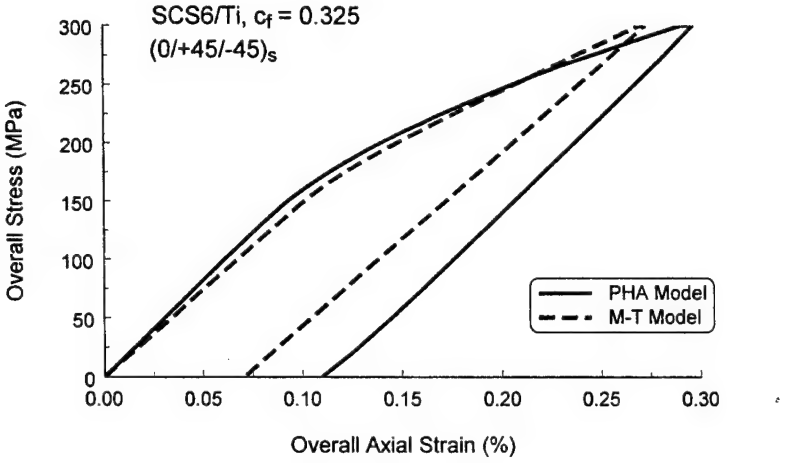

Figure 15 Overall axial strain computed for a high-temperature metal matrix laminate subjected to the load history of Figure 14.

1.14.5.4 Application

The methods described above have been used to evaluate the overall strains and fiber axial stress in a silicon carbide-titanium, $(0/\pm45)_s$ laminate caused by in-plane normal and shear stresses applied in a proportional path at 565 °C (Bahei-El-Din *et al.*, 1998). The load-time record is shown in Figure 14. Material properties of the elastic Sigma fiber and the viscoplastic Timetal-21S matrix provided by Bahei-El-Din and Dvorak (1997) are used, and a fiber volume fraction of 0.325 is assumed.

The computed axial and shear strains are plotted in Figure 15 and 16, and the axial fiber stress in the 0°-ply is shown in Figure 17. The figures compare the predictions obtained with the Mori–Tanaka averaging model and the periodic hexagonal array model. In the latter, a refined mesh of the unit cell with 48 matrix elements and 24 fiber elements was used for each ply. It is seen that averaging the local fields over the fiber and matrix phases, as modeled by the Mori–Tanaka scheme, underestimates the overall strains and the fiber stress in comparison with the more refined representation of the local fields offered by the finite element solution of the PHA unit cell. Since axial deformation of the laminate is dominated by the elastic 0°-fiber, the Mori–Tanaka estimates of the laminate maximum axial strain and fiber axial stress in the 0°-ply are smaller than the finite element estimates by only 10%. In contrast, a much stiffer shear response is obtained with the Mori–Tanaka model leading to an estimated laminate maximum shear strain that is smaller than the finite element value by 60%.

1.14.6 CLOSURE

Although efforts to estimate the overall elastic moduli of composite aggregates from local properties date back to the early 1960s,

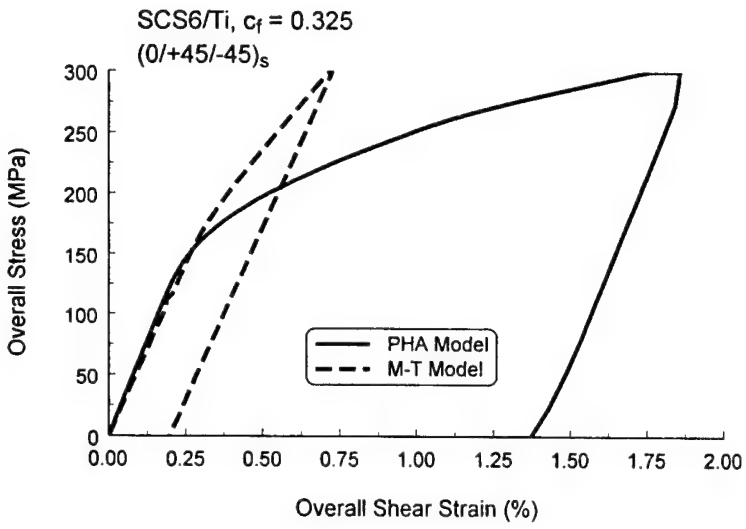

Figure 16 Overall shear strain computed for a high-temperature metal matrix laminate subjected to the load history of Figure 14.

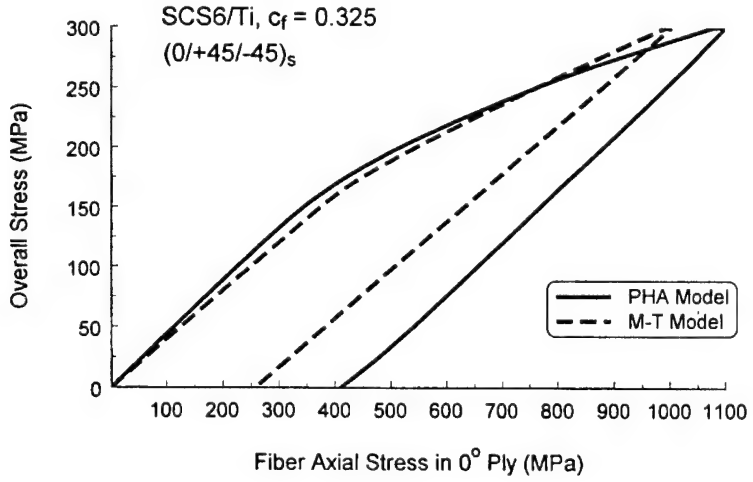

Figure 17 Fiber axial stress computed in the 0°-ply of a high-temperature metal matrix laminate subjected to the load history of Figure 14.

development of micromechanical theories for inelastic composite materials has seen major advances only in recent years. These have been summarized in this chapter with emphasis on fibrous composites with phases that exhibit plastic and viscoplastic deformation. Capabilities of the analytical methods developed for these composite systems in predicting their overall response under thermomechanical loads have been also illustrated.

The methods discussed center on evaluation of local stress and strain concentration factors that reflect interactions of the phases and their *in situ* constitutive behavior. Two classes of micromechanical models can be utilized in computing the concentration factors, averaging models, which derive phase interactions from solution of certain inclusion problems without specific reference to the microgeometry, and periodic array models, which derive phase interactions from an idealized geometry of the microstructure. Representation of the local fields in these two models is quite different. In averaging models, the local fields are averaged over each phase, and thus the local phase properties are assumed to be homogeneous within the phase. Although valid for elastic phases, this assumption may lead to large errors in the predicted overall response when behavior of the phases is nonlinear. In periodic array models, a piecewise uniform field is selected with a desired level of refinement. This is expected to provide more realistic predictions, albeit at a higher computational effort.

In plasticity, formulation of the governing equations for the local stresses may proceed in

two different ways. In one method, the formulation follows that of elastic inclusion problems, leading to averaging models, but with instantaneous phase properties. The second method, known as transformation field analysis, finds the local fields by superposition of the fields caused by the overall loads, and the local transformation strains. The method is applicable to both averaging and periodic models, and requires derivation of only elastic concentration and transformation factors.

Viscoplastic analysis for either averaging or periodic models with the transformation field method leads to closed-form rate equations for the local discrete stress field. These equations have been expanded to include the stresses in various plies of a laminated structure. The resulting equations reflect interaction of the phases in the individual plies, and mutual constraints caused by bonding the plies together.

While the focus in the present summary of nonlinear analysis of composites was on micromechanical models, other related techniques for evaluation of the overall response can be found in the literature. For example, several variational methods for estimating effective behavior of nonlinear composites with random microstructures have been developed in the past 15 years. In elasticity, this line of inquiry was initiated by Hashin and Shtrikman (1962, 1963) who used special forms of classical variational principles of elasticity, together with certain polarization fields in a homogeneous comparison medium, to obtain rigorous bounds on the effective elastic stiffness tensor of statistically homogeneous composites. Generalization of the Hashin–Shtrikman variational principles to nonlinear elastic composites was first proposed by Talbot and Willis (1985). New variational principles using a linear comparison composite were later developed by Ponte Castaneda (1992), and by Suquet (1983) for power-law composites. Several other procedures and more recent developments of variational methods have been reviewed and summarized by Suquet (1997) and Ponte Castaneda and Suquet (1998).

Although they offer rigorous estimates of effective properties in certain special circumstances, the variational methods are based on and thus limited to systems exhibiting nonlinear elastic or viscous material behavior. Some extensions have been made to power-law materials and incremental theory of plasticity. Also, general agreement of the variational model predictions has been found with the bimodal yield surfaces of Section 1.14.3.3 (deBotton, 1995). However, much more work is needed before more complex inelastic material behavior, which is implied by available experiments discussed, for example, in Section 1.14.3.4, can be represented, especially under a variable loading–unloading regime.

Despite the progress witnessed in micromechanics of nonlinear composite materials, there are several unresolved issues that deserve future attention. So far, constitutive behavior of the matrix has been measured from specimens prepared from bulk material. This could be different from *in situ* behavior of the matrix, which is constrained by the reinforcement. Moreover, processing under high temperature and pressure may cause a significant change in the local properties. Damage, in the form of interface decohesion, or microcracks in the phases are often observed in composites after fabrication or application of service loads, and could be coupled with plastic or viscoplastic flow of the phases. Finally, although periodic models provide reliable estimates of the overall inelastic properties, it may not be representative of certain composite systems. In this case, averaging models or variational techniques can be applied but in certain cases may deliver unreliable predictions. Macromechanical models represent an alternative, but do not have the versatility of micromechanics.

ACKNOWLEDGMENTS

The work presented in this chapter was supported by grants from Ship Structures & Systems S&T Division, Mechanics Division of the Office of Naval Research, Engineering and Environmental Sciences Division, and Solid Mechanics Program of the US Army Research Office. Drs. Yapa Rajapakse and Kailasam Iyer served as program monitors.

1.14.7 REFERENCES

Y. A. Bahei-El-Din, in 'Thermal and Mechanical Behavior of Metal Matrix and Ceramic Matrix Composites', eds. J. M. Kennedy, H. H. Moeller and W. S. Johnson, ASTM, Philadelphia, PA, STP 1080, 1990, pp. 20–39.

Y. A. Bahei-El-Din, in 'VISCOPAC Finite Element Program for Viscoplastic Analysis of Composites, User's Manual', Structural Engineering Department, Cairo University, Egypt, 1994.

Y. A. Bahei-El-Din, *Int. J. Plasticity*, 1992, **8**, 867–892.

Y. A. Bahei-El-Din, *Mech. Composite Mater. Structures*, 1996, **3**, 1–28.

Y. A. Bahei-El-Din and G. J. Dvorak, *Mech. Composite Mater. Structures*, 1997, **4**, 131–158.

Y. A. Bahei-El-Din, G. J. Dvorak and S. Utku, *Computers and Structures*, 1981, **13**, 321–330.

Y. A. Bahei-El-Din, I. A. Ibrahim and A. G. Botrous, in 'IUTAM Symposium on Transformation Problems in Composite and Active Materials', eds. Y. A. Bahei-El-Din and G. J. Dvorak, Kluwer Academic Publishers,

Dordrecht, 1998, pp. 45–60.
Y. A. Bahei-El-Din, R. S. Shah and G. J. Dvorak, in 'Mechanics of Composites at Elevated and Cryogenic Temperatures', eds. S.N. Singhal, W.F. Jones, T. Cruse and C.T. Herakovich, ASME, New York, 1991, AMD-vol. 118, pp. 67–78.
Y. Benveniste, *Mech. Mater.*, 1987, **6**, 147–157.
S. R. Bodner and Y. Partom, *J. Appl. Mech.*, 1975, **42**, 385.
J. R. Brockenbrough, S. Suresh and H. A. Wienecke, *Acta Metall Mater.*, 1991, **39**, 735–752.
B. Budiansky, *J. Mech. Phys. Solids*, 1965, **13**, 223–227.
V. Buryachenko, *Acta Mech.*, 1996, **119**, 93–117.
J. L. Chaboche, *Int. J. Plasticity*, 1989, **5**, 247–302.
T. Y. Chen, G. J. Dvorak and Y. Benveniste, *J. Appl. Mech.*, 1992, **59**, 539–546.
R. M. Christensen, 'Mechanics of Composite Materials', John Wiley and Sons, New York, 1979.
Y. F. Dafalias and E. P. Popov, *J. Appl. Mech.*, 1976, **43**, 645–651.
G. deBotton, *Int. J. Solids Structures*, 1995, **32**, 1743–1757.
D. C. Drucker, in 'Proceedings of the First U.S. National Congress of Applied Mechanics', ASME, New York 1952, p. 487.
G. J. Dvorak, in 'Metal Matrix Composites, Mechanisms and Properties', eds. R. K. Everett and R. J. Arsenault, Academic Press, Boston, MA, 1991, p. 1–77.
G. J. Dvorak, *Proc. R. Soc. Lond.*, 1992, **A437**, 311–327.
G. J. Dvorak and Y. A. Bahei-El-Din, *J. Appl. Mech.*, 1982, **49**, 327–335.
G. J. Dvorak and Y. A. Bahei-El-Din, *Acta Mechanica*, 1987, **69**, 219–241.
G. J. Dvorak and Y. A. Bahei-El-Din, in 'IUTAM Symposium on Microstructure-Property Interactions in Composite Materials', ed. R. Pyrz, Kluwer, Dordrecht, 1995, pp. 89–100.
G. J. Dvorak, Y. A. Bahei-El-Din, Y. Macheret and C. H. Liu, *J. Mech. Phys. Solids*, 1988, **36**, 655–687.
G. J. Dvorak, Y. A. Bahei-El-Din and A. M. Wafa, *Computational Mechanics*, 1994, **14**, 201–228.
G. J. Dvorak and Y. Benveniste, *Proc. R. Soc. Lond.*, 1992, **A437**, 291–310.
G. J. Dvorak and J. L. Teply, in 'Plasticity Today: Modeling, Methods, and Applications, W. Olszak Memorial', eds. A. Sawczuk and G. Bianchi, Elsevier Science Publishers, Amsterdam, 1985, pp. 623–642.
M. A. Eisenberg and C. F. Yen, *J. Appl. Mech.*, 1981, **48**, 276–284.
J. D. Eshelby, *Proc. R. Soc. Lond.*, 1957, **A241**, 376–396.
F. Ghahremani, *Mech. Res. Commun.*, 1977, **4**, 89.
Z. Hashin and S. Shtrikman, *J. Mech. Phys. Solids*, 1962, **10**, 335–342.
Z. Hashin and S. Shtrikman, *J. Mech. Phys. Solids*, 1963, **11**, 127–140.
R. Hill, *J. Mech. Phys. Solids*, 1963, **11**, 357–372.
R. Hill, *J. Mech. Phys. Solids*, 1964, **12**, 199–212.
R. Hill, *J. Mech. Phys. Solids*, 1965a, **13**, 189–198.
R. Hill, *J. Mech. Phys. Solids*, 1965b, **13**, 213–222.
T. Iwakuma and S. Nemat-Nasser, *Composites and Structures*, 1983, **16**, 13–19.
W. S. Johnson, M. Mirdamadi and Y. A. Bahei-El-Din, *J. Composites Tech. Res.*, 1993, **15**, 297–303.
N. Kinoshita and T. Mura, *Physica Status Solidi A*, 1971, **5**, 759–768.
D. C. Lagoudas, A. C. Gavazzi and H. Nigam, *Computational Mechanics*, 1991, **8**, 193.
V. M. Levin, *Mech. of Solids*, 1967, **2**, 58–61.
M. C. M. Liu and E. Krempl, *J. Mech. Phys. Solids*, 1979, **27**, 377.
T. Mori and K. Tanaka, *Acta Metall.*, 1973, **21**, 571–574.
H. Moulinec and P. Suquet, *C.R. Acad. Sci. Paris Serie II*, 1994, **318**, 1417–1423.
T. Mura, 'Micromechanics of Defects in Solids', Martinus Nijhoff Publishers, The Hague, 1982.
S. Nemat-Nasser and M. Hori, 'Micromechanics: Overall Properties of Heterogeneous Materials', Elsevier Science Publishers, Amsterdam, 1993.
R. W. Neu, in 'Material Parameter Estimation for Modern Constitutive Equations', eds. L. A. Bertram, S. B. Brown and A. D. Freed, ASME, New York, 1993, MD-vol. 43/AMD-vol. 168, pp. 211–226.
H. Nigam, G. J. Dvorak and Y. A. Bahei-El-Din, *Int. J. Plasticity*, 1994a, **10**, 23–48.
H. Nigam, G. J. Dvorak and Y. A. Bahei-El-Din, *Int. J. Plasticity*, 1994b, **10**, 49–62.
A. Phillips and C. W. Lee, *Int. J. Solids Structures*, 1979, **15**, 715–729.
A. Phillips, C. S. Liu and J. W. Justusson, *Acta Mechanica*, 1972, **14**, 119.
A. Phillips and H. Moon, *Acta Mechanica*, 1977, **27**, 91–102.
P. Ponte Castaneda, *J. Mech. Phys. Solids*, 1992, **40**, 1757–1788.
P. Ponte Castaneda and P. Suquet, in 'Advances in Applied Mechanics', Academic Press, New York, 1998, pp. 171–302.
W. Prager, *Proc. Inst. Mech. Engrs.*, 1955, **41**, 169.
P. Suquet, *C.R. Acad. Sci. Paris Serie II*, 1983, **296**, 1355–1358.
P. Suquet, in 'Continuum Micromechanics', ed. P. Suquet, Springer-Verlag, Wien, 1997, pp. 197–264.
D. R. S. Talbot and J. R. Willis, *J. Appl. Math.*, 1985, **35**, 39–54.
J. L. Teply and G. J. Dvorak, *J. Mech. Phys. Solids*, 1988, **36**, 29–58.
A.M. Wafa, Ph.D. Thesis, Rensselaer Polytechnic Institute, Troy, NY, 1994.
K. P. Walker, 'Research and Development Program for Nonlinear Structural Modeling with Advanced time-Dependent Constitutive Relationships', NASA Lewis Research Center, Report No. CR-165 533, 1981.
K. P. Walker, A. D. Freed and E. H. Jordan, *Comp. Sci. Tech.*, 1994, **50**, 71–84.
L. J. Walpole, *Proc. Roy. Soc. London*, 1967, **A300**, 270.
L. J. Walpole, *J. Mech. Phys. Solids*, 1969, **17**, 235.
H. Ziegler, *Q. Appl. Math.*, 1959, **17**, 55.

1.14.8 APPENDIX

Here, we record some results related to estimates of the overall moduli of fibrous composites using averaging models. Both the fiber and matrix are assumed to be transversely isotropic with x_1 as the axis of rotational symmetry. Let E_L and E_T denote, respectively, the longitudinal and transverse elastic Young's modulus, and ν_L and ν_T denote Poisson's ratios under axial and transverse straining. Similarly, we denote the longitudinal and transverse elastic shear moduli by G_L and G_T. The elastic stress–strain relation $\boldsymbol{\varepsilon} = \mathbf{M}\boldsymbol{\sigma}$ for either phase, where $\mathbf{M}$ is the elastic compliance matrix, is written using the engineering moduli as

$$\begin{Bmatrix} \varepsilon_{11} \\ \varepsilon_{22} \\ \varepsilon_{33} \\ 2\varepsilon_{23} \\ 2\varepsilon_{31} \\ 2\varepsilon_{12} \end{Bmatrix} = \begin{bmatrix} 1/E_L & -\nu_L/E_L & -\nu_L/E_L & 0 & 0 & 0 \\ & 1/E_T & -\nu_T/E_T & 0 & 0 & 0 \\ & & 1/E_T & 0 & 0 & 0 \\ & & & 1/G_T & 0 & 0 \\ & SYM. & & & 1/G_L & 0 \\ & & & & & 1/G_L \end{bmatrix} \begin{Bmatrix} \sigma_{11} \\ \sigma_{22} \\ \sigma_{33} \\ \sigma_{23} \\ \sigma_{31} \\ \sigma_{12} \end{Bmatrix} \tag{125}$$

The stiffness $\mathbf{L} = \mathbf{M}^{-1}$ is best written in terms of Hill's (1964) moduli,

$$k = -\left[1/G_T - 4/E_T + 4\nu_L^2/E_L\right]^{-1}, \ell = 2k\nu_L$$
$$n = E_L + 4k\nu_L^2 = E_L + \ell^2/k, m = G_T, p = G_L \tag{126}$$

The constitutive relation $\boldsymbol{\sigma} = \mathbf{L}\boldsymbol{\varepsilon}$ is then written as

$$\begin{Bmatrix} \sigma_{11} \\ \sigma_{22} \\ \sigma_{33} \\ \sigma_{23} \\ \sigma_{31} \\ \sigma_{12} \end{Bmatrix} = \begin{bmatrix} n & \ell & \ell & 0 & 0 & 0 \\ & (k+m) & (k-m) & 0 & 0 & 0 \\ & & (k+m) & 0 & 0 & 0 \\ & & & m & 0 & 0 \\ & SYM. & & & p & 0 \\ & & & & & p \end{bmatrix} \begin{Bmatrix} \varepsilon_{11} \\ \varepsilon_{22} \\ \varepsilon_{33} \\ 2\varepsilon_{23} \\ 2\varepsilon_{31} \\ 2\varepsilon_{12} \end{Bmatrix}. \tag{127}$$

We recall that Hill's formulation of the Eshelby's inclusion problem, Section 1.14.2.2.1, provides the strain and stress concentration factors in the fiber and matrix in terms of matrices **P** and **Q**. These matrices depend on the shape of the ellipsoidal inclusion and elastic moduli of the matrix, and are related by Equation (20). For continuous fibers of a circular cross section embedded in a transversely isotropic matrix, the nonzero components of **P** are given by

$$P_{22} = P_{33} = \frac{k_1 + 4m_1}{8m_1(k_1 + m_1)}$$
$$P_{23} = P_{32} = \frac{-k_1}{8m_1(k_1 + m_1)} \tag{128}$$
$$P_{44} = P_{55} = \frac{1}{2p_1}, \qquad P_{66} = \frac{k_1 + 2m_1}{2m_1(k_1 + m_1)}$$

where k_1, m_1, and p_1 are Hill's elastic moduli of the matrix phase.

Estimates of the overall moduli of binary composite materials by the self-consistent method are found by replacing the matrix moduli in Equation (128) by the effective moduli of the composite aggregate, and substituting the result in Equation (22). This provides the concentration factors, which are then substituted in Equation (6) to determine the overall moduli. Numerical values of the overall Hill's moduli m, p and k are computed from the following uncoupled equations (Hill, 1965a, 1965b),

$$\frac{c_f k_f}{k_f + m} + \frac{c_m k_m}{k_m + m} = 2\left[\frac{c_f m_m}{m_m - m} + \frac{c_m m_f}{m_f - m}\right] \tag{129}$$

$$\frac{1}{2p} = \frac{c_f}{p - p_m} + \frac{c_m}{p - p_f}, \frac{1}{k + m} = \frac{c_f}{k_f + m} + \frac{c_m}{k_m + m} \tag{130}$$

Here, c_f and c_m are volume fractions of the fiber and matrix, and m_r, p_r, and k_r, $r = f,m$, are Hill's moduli of the phases. The remaining two moduli, ℓ and n, are found from the universal connections

$$\frac{k - k_f}{\ell - \ell_f} = \frac{k - k_m}{\ell - \ell_m} = \frac{\ell - c_f\ell_f - c_m\ell_m}{n - c_f n_f - c_m n_m} = \frac{k_f - k_m}{\ell_f - \ell_m} \tag{131}$$

The Mori–Tanaka model, on the other hand, utilizes the form of matrix **P** given in Equation (128) to compute partial concentration factors, which provide the fiber average stress and strain in terms of their matrix counterparts, Equations (23) and (24). The overall moduli are then found from Equations (6), (23)–(26). Chen *et al.* (1992) give the Mori–Tanaka moduli for fibrous composites in the following explicit form,

$$p = \frac{2c_f p_m p_f + c_m\left(p_m p_f + p_m^2\right)}{2c_f p_m + c_m\left(p_f + p_m\right)} \tag{132}$$

$$m = \frac{m_m m_f(k_m + 2m_m) + k_m m_m\left(c_f m_f + c_m m_m\right)}{k_m m_m + (k_m + 2m_m)\left(c_f m_m + c_m m_f\right)} \tag{133}$$

$$k = \frac{c_f k_f(k_m + m_m) + c_m k_m\left(k_f + m_m\right)}{c_f(k_m + m_m) + c_m\left(k_f + m_m\right)} \tag{134}$$

$$\ell = \frac{c_f \ell_f(k_m + m_m) + c_m \ell_m\left(k_f + m_m\right)}{c_f(k_m + m_m) + c_m\left(k_f + m_m\right)} \tag{135}$$

$$n = c_m n_m + c_f n_f + \left(1 - c_f\ell_f - c_m\ell_m\right)\frac{\ell_f - \ell_m}{k_f - k_m} \tag{136}$$

For completeness, we record the overall Hill's moduli estimated with the vanishing fiber diameter model (Dvorak and Bahei-

El-Din, 1982; Bahei-El-Din, 1990). In this model, the fiber constrains the matrix deformation in the axial direction only. Consequently, unit strain concentration factors are assumed under axial straining, and unit stress concentration factors are assumed under transverse normal and shear stresses as well as longitudinal shear stress. The result is

$$p = \frac{p_m p_f}{c_f p_m + c_m p_f} \qquad m = \frac{m_m m_f}{c_f m_m + c_m m_f} \tag{137}$$

$$k = \frac{k_m k_f}{c_f k_m + c_m k_f} \qquad \ell = \frac{c_f \ell_f k_m + c_m \ell_m k_f}{c_f k_m + c_m k_f} \tag{138}$$

$$n = c_m n_m + c_f n_f - \frac{c_f c_m (\ell_f - \ell_m)^2}{c_f k_m + c_m k_f} \tag{139}$$